Mechanical and Chloride Transport Performance of Particle Size Classified Limestone Blends

by

Matthew Aguayo

A Thesis Presented in Partial Fulfillment
of the Requirements for the Degree
Master of Science

Approved April 2014 by the
Graduate Supervisory Committee:

Narayanan Neithalath, Chair
Barzin Mobasher
Subramaniam Rajan

ARIZONA STATE UNIVERSITY

May 2014

ABSTRACT

The demand for portland cement concrete is expected to increase over time. There is a need to develop a more sustainable cementitious systems in order to reduce the negative environmental impacts associated with ordinary portland cement (OPC) production. An attempt is made to investigate sustainable binder solutions through the use of alternative cementitious materials at high levels of volume replacement. Limestone, an abundant material is used as a filler in low water-to-powder concretes where a substantial fraction of the portland cement remains unhydrated. At high volume OPC replacement, 20% and 35%, the combination of limestone and an alumina source has been shown to improve mechanical and durability performance. At 20% OPC replacement levels the migration coefficient which is an indication of chloride penetration in concrete is lower than the OPC control mixture at 28 and 56 days of hydration. The use of limestone with a similar particle size distribution to that of the OPC is used in each of these blended systems. A 20% binary limestone blend provide similar strength to an OPC mortar at all ages and comparable transport properties to that of the OPC concrete. Fly ash and metakaolin are the two alumina sources for the ternary blended mixes with concrete. The metakaolin shows the highest increase in the amount of hydration products formed out of all the mixes, including calcium-silicate-hydrate and carboaluminate phases in combination with limestone powder. At both levels of replacement the metakaolin blends show a substantially lower migration coefficient which is contributed to the smaller pore sizes found in the metakaolin blends. The fracture response of these systems show that at all replacement levels the ductility of the systems increase indicated by the large critical crack tip opening displacement. The fracture toughness is the highest for the blend containing metakaolin

indicative of the smaller pore sizes allowing more dissipation of energy. An attempt is made to relate all mechanical and durability parameters to the reaction products and pore-structure developing at later ages.

ACKNOWLEDGEMENTS

I would first like to thank my daughter Brynn for being my greatest motivation to never give up in life, Elizabeth, my parents, brother, and family who have always supported me and my goals in life. No words can express how much your love and encouragement has brought out the best in me.

I would like to thank Dr. Narayanan Neithalath for his guidance, support, and exposing me to the benefits and struggles of performing sustainable and fundamental material based research. I appreciate your encouragement and enthusiasm through the completion of my master's degree. I would also like to thank my committee members Dr. Subramaniam Rajan and Dr. Barzin Mobasher for taking the time to examine my thesis.

I would like to thank my lab mates, Akash, Aashay, Sumanta, Sateesh, Pu, Shannon, and every other student in our structures and materials group for all their help and guidance during completion of my thesis. A special thanks is given to my mentor and the best person I could have ever met during my undergraduate and graduate research experience, Kirk. Your guidance and ability to answer any and all of my questions and doubts have made my experience in research the best I could have ever asked for and I am extremely grateful.

Finally I would like to thank Arizona State University and the School of Sustainable Engineering and the Built Environment for providing me with the resources required to complete my M.S. in Civil Engineering.

TABLE OF CONTENTS

Page

CHAPTER Page

CHAPTER Page

LIST OF TABLES

Table Page

LIST OF FIGURES

Figure Page

Figure Page

Figure Page

1. INTRODUCTION

Portland cement concrete (PCC) plays an immense role in today's building and transportation infrastructure as the major structural component of most bridges (including the bridge deck, abutments, and piers), roadways in freezing climates, airport pavements, and commercial buildings. The main binding component in PCC, ordinary portland cement (OPC) requires significant energy, and emits significant quantities of the greenhouse gas CO_2 as a product of energy production as well as due to the chemical reactions associated with production of the clinker (about 0.8 tons per ton of OPC produced (Ali, Saidur, & Hossain, 2011)). Portland cement production has been shown to account for approximately (5%) (Hendriks, Worrell, De Jager, Blok, & Riemer, 2002; Rehan & Nehdi, 2005; E. Worrell, 2014; Ernst Worrell, Martin, & Price, 2000) of global carbon dioxide emissions. This reduces the sustainability of PCC as a structural material. Further, it has been noted that the demand for PCC is expected to continue to increase over the coming decades (Imbabi, Carrigan, & McKenna, 2012; Oggioni, Riccardi, & Toninelli, 2011), indicating this is an ideal time to focus on increasing the sustainability of this material. Advances in sustainable PCC technology thus far have resulted in a limited decrease in CO_2 emissions and energy consumption per unit volume of concrete produced (Aranda Usón, López-Sabirón, Ferreira, & Llera Sastresa, 2013; Bentz, Hansen, & Guynn, 2011; Schneider, Romer, Tschudin, & Bolio, 2011; Z. Zhang, Provis, Reid, & Wang, 2014). These advances have primarily been focused on the use of waste/by-product materials from other industries, providing the combined benefit in reduction in landfilled material, increasing the durability and strength of PCC, and decreasing the total quantity of portland cement required (Imbabi et al., 2012; Oggioni et al., 2011; Rehan & Nehdi, 2005). The waste stream materials used

commonly include fly ash from coal production and blast furnace slag from steel production. However, there is a limited supply of these waste stream materials, and the availability of these materials, fly ash in particular, are expected to decrease in United States over the coming decades due to the increased use of natural gas for energy production. These facts, combined with the exceptionally high volume of concrete produced globally, indicates that these traditional replacement methods are unlikely to allow for high volume cement replacement which would allow for a significant global reduction in portland cement demand. Given the high volume of concrete produced, enhancement of PCC sustainability requires the use of an abundant replacement material, perhaps in combination with industrial waste stream materials to allow for a significant reduction in global demand. It is, however, critical that the mechanical and durability properties of these materials be comparable to, or better than PCC, which will allow for industrial acceptance and implementation. One such replacement material that has garnered significant interest in recent years (Bentz, Sato, de la Varga, & Weiss, 2012; V. Bonavetti, Donza, Menéndez, Cabrera, & Irassar, 2003; D P Bentz, 2009; De Weerdt, Haha, et al., 2011; Lothenbach, Le Saout, Gallucci, & Scrivener, 2008; Marzouki, Lecomte, Beddey, Diliberto, & Ben Ouezdou, 2013; Matschei, Lothenbach, & Glasser, 2007; Oey, Kumar, Bullard, Neithalath, & Sant, 2013; Vance, Aguayo, Oey, Sant, & Neithalath, 2013), is limestone which is both inexpensive and widely available.

Determination of the mechanical and durability characteristics of novel cementitious binder systems is critical to the development and industrial acceptance of these materials. In this study portland cement replacement levels of 20% and 35% (volume basis) are used to proportion binary and ternary blends containing limestone, fly ash, and metakaolin to

observe possible synergistic benefits on durability and fracture performance of these materials. The limestone powder has been blended to have a comparable particle size distribution to portland cement eliminating the effect of particle packing as a cause of determined phenomena. This was accomplished using least squares fitting of limestone powder of several median particle sizes to achieve the desired distribution. The two test methods for evaluating the chloride ingress are the rapid chloride permeability (RCP) and non-steady-state migration (NSSM) ("ASTM C1202 - 12. Standard Test Method for Electrical Indication of Concrete's Ability to Resist Chloride Ion Penetration," 2012, "NT Build 492. Concrete, Mortar and Cement-Based Repair Materials: Chloride Migration Coeffecient from Non-Steady-State Migration Experiments," 1990). Electrical impedance spectroscopy studies have been performed on the specimens before and after the NSSM test to measure the bulk resistance giving an indication on how the microstructure is developing in these different systems. The quantity and type of hydration products influencing the pore structure and connectivity for the different supplementary cementitious materials is characterized through thermogravimetric analysis (TGA). Mercury intrusion porosimetry (MIP) was performed to analyze and quantify the pore structure characteristics of the different binary and ternary blends. The fracture parameters will be characterized using the two-parameter fracture model on notched beams subjected to three-point bending (Jenq & Shah, 1985). From the two-parameter model the fracture toughness and critical crack tip opening displacement ($CTOD_c$) will be determined and a comparison made between different levels of volume replacement.

1.1. Objectives

The objectives of this study are listed below:

i. Understand and explore possible synergistic benefits of combining alumina sources with limestone as cement replacement. To disconnect the influence of particle packing and limestone fineness via the use of limestone particle size distributions which closely match that of OPC.

ii. Provide a better understanding on the fundamental behavior of limestone in combination with alternative cementitious materials (ACM) within the context of mechanical performance, chemical reactivity, and durability characteristics.

1.2. Thesis Layout

Chapter 2 provides a literature review of previous studies on alternative increasing concrete sustainability through cement replacement, with a primary focus on the use of limestone, and possible synergistic benefits of limestone replacement in combination with an alumina source such as fly ash or metakaolin. The influence of limestone powder on cement hydration, compressive strength, and other key factors are explored. A review of the work that has been previously completed on concrete durability is explored, with a focus on ionic transport. Finally, an exploration of a fracture mechanics approach to analyzing concrete is also discussed.

Chapter 3 will detail the experimental design, mixture proportions, and testing procedures for microstructural characterization, mechanical and durability performance.

Chapter 4 discusses the mechanical performance of ternary blend concretes through the compressive strength behavior and fracture mechanics approach.

Chapter 5 will provide an analysis on the ionic transport of ternary blend concretes evaluated through two chloride ion transport test methods.

Chapter 6 concludes with a concise summary and explanation of the observed results from the chemical, physical, and durability aspects.

2. LITERATURE REVIEW

2.1. Background and Overview

Portland cement concrete is composed of aggregates, portland cement paste, and water. The primary mechanism of material deterioration in reinforced concrete is chloride ion ingress which initiates steel reinforcement corrosion. This resultant corrosion has been shown to be a significant cost in infrastructure repair and rehabilitation, costing approximately $23 billion annually in infrastructure repairs (FHWA, 2002). This corrosion results in a volume increase in the reinforcing steel which subsequently results in cracking and spalling of the concrete. This cracking then results in increased ion penetration into the concrete, further enhancing reinforcement corrosion (Almusallam, 2001; Capozucca, 1995; Fang, Lundgren, Chen, & Zhu, 2004). Chloride ion penetration is a diffusion process, which is dominated by the pore structure of the material, with more porous materials allowing for easier diffusion of chloride ions into the concrete. As the hardened cement paste is typically significantly more porous than the aggregate present in the concrete, diffusion primarily happens through the cement paste, or binding component in the concrete (Balonis, Lothenbach, Le Saout, & Glasser, 2010; Díaz, Nóvoa, & Pérez, 2006; Garboczi, 1990). Supplementary cementitious materials (SCM) such as fly ash and slag have been shown to refine the pore structure of the cement paste at later ages (Bentz et al., 2012; R. Feldman, Prudencio Jr., & Chan, 1999; Githachuri & Alexander, 2013; J. A. Jain & Neithalath, 2010; Luo, Cai, Wang, & Huang, 2003), decreasing mean pore size in the microstructure , which decreases the ability of ions to diffuse into the concrete and initiate corrosion. However, the limited availability of these materials give rise the need for the use of other more widely available materials in an effort to produce a more sustainable

concrete, one such material is limestone powder. The current study is focused on the investigation of the microstructural changes of limestone cement systems, and limestone blends including additional alumina sources, and specifically targeting ion transport phenomena and fracture response in these systems.

2.2. Synergies between Limestone, Fly Ash, and Metakaolin

The use of limestone (LS) in cement has been widely investigated in recent decades, with the general conclusion that limestone replacement of cement results in a strength reduction of the concrete (Domone, 2007; Ghrici, Kenai, & Said-Mansour, 2007; Khatri, Sirivivatnanon, & Gross, 1995; Menéndez, Bonavetti, & Irassar, 2003), acceleration of the hydration reaction (V. Bonavetti et al., 2003; Darweesh, 2004; Lothenbach et al., 2008; Oey et al., 2013), decreased setting time (Bentz et al., 2012; Irassar et al., 2011; Pelletier-Chaignat, Winnefeld, Lothenbach, & Müller, 2012; Shoude, Cheng, Lingchao, & Xin, 2012), and in some cases decreased porosity of the resultant hardened paste (Chen, Kwan, & Jiang, 2014; Courard & Michel, 2014; Pipilikaki & Beazi-Katsioti, 2009). These results have been shown to be largely dependent on the size of limestone used in the study (Bentz et al., 2012; Cam & Neithalath, 2010; Oey et al., 2013; Vance et al., 2013), with finer limestone generally showing better performance from the above listed perspectives, while coarser limestone is seen to act more as a traditional filler. Limestone in cementitious systems has been shown to react to some extent with the alumina phases in cement (Darweesh, 2004; Pelletier-Chaignat et al., 2012; Shoude et al., 2012), as well as provide a nucleation site for hydration products. Based on this interaction with the alumina phase, it has been proposed that there may be a synergistic benefit of inclusion of additional alumina sources in portland cement systems (De Weerdt, Kjellsen, Sellevold, & Justnes,

2011; Githachuri & Alexander, 2013; Menéndez et al., 2003; Vance et al., 2013). The combined use of SCMs and limestone powder has been investigated primarily in the context of early age behavior of these systems, including rheological characterization, and influences on hydration kinetics (De Weerdt, Haha, et al., 2011; Lothenbach et al., 2008; Vance et al., 2013). It has been shown that limestone in the presence of an aluminate species leads to an increase in the volume of hydrates and naturally a decrease in porosity (Antoni, Rossen, Martirena, & Scrivener, 2012; De Weerdt, Kjellsen, et al., 2011) as compared to binary systems of portland cement and limestone. Decreasing the porosity of these systems results in a strength increase as compared to the binary systems, which indicates a synergistic benefit offsetting some of the strength reduction associated with limestone replacement.

2.2.1. Fly Ash

Class F fly ash (FA) also known as a low calcium fly ash is a by-product of coal fired electric power plants. It has been documented that FA improves the durability and lowers the heat of hydration when used as a cement replacement (Nochaiya, Wongkeo, & Chaipanich, 2010). However, it is notable that the pozzolanic reaction of fly ash is a slow process, and thus the effects of FA on early age reaction kinetics, setting, and strength development is not significant. In order to compensate for the delay in durability and mechanical properties limestone blended with the fly ash provides accelerated early age property development (Bentz et al., 2012). At later ages this pozzolanic reaction of fly ash within blended limestone cements has been shown to improve the durability properties by refining the pore structure, as the alumina and siliceous phases react with the portlandite in portland cement to form new hydration products. The hydration products or binding phases

formed in fly ash-cement based systems are calcium silicate hydrates (C-S-H) where the pozzolanic reaction consumes portlandite in the cement (Richardson, 1999) or in alkali activated systems where sodium aluminosilicates (N-A-S-H) and aluminum modified calcium silicate hydrates (C-A-S-H) (Garcia-Lodeiro, Palomo, Fernández-Jiménez, & Macphee, 2011) are formed by the higher alkalinity initially present in the system. The influence of limestone in fly ash systems is that an increase in the volume of hydration products arises when the alumina species in fly ash reacts with the calcium in limestone to form carboaluminate phases while at the same time stabilizing the formation of ettringite (K. Celik et al., 2014).

2.2.2. Metakaolin

Metakaolin (MK) is a pozzolan produced by the thermal processing of kaolin clay (Gruber, Ramlochan, Boddy, Hooton, & Thomas, 2001). Metakaolin has amorphous structure consisting mostly of aluminosilicates, and forms a cementitious structure when combined with calcium hydroxide. Similar to fly ash the alumina present in metakaolin reacts with calcium in the limestone to form carboaluminate phases. Metakaolin has been shown to be more reactive than fly ash and other pozzolanic materials due to the higher surface area and greater alumina species (Poon, Lam, Kou, Wong, & Wong, 2001). The higher reactivity leads to more consumption of calcium hydroxide increasing the amount of hydration products, refining the pore structure, and improving mechanical and durability performance (Antoni et al., 2012; Kadri, Kenai, Ezziane, Siddique, & De Schutter, 2011; Paiva, Velosa, Cachim, & Ferreira, 2012; Poon et al., 2001; Shekarchi, Bonakdar, Bakhshi, Mirdamadi, & Mobasher, 2010; Vance et al., 2013).

2.3. Particle Size Matching

There are some researchers who are developing models that can predict the hydration reactions and compressive development by varying the degrees of fineness in limestone powders in relation with a given control mix (Kumar et al., 2013). The idea is to tailor the material in such a way as to predict and measure the performance with an accurate model. The fineness and dosage of limestone powder greatly influences the hydration process. By using a limestone finer than OPC, it has been found that the limestone will provide nucleation sites, and enhance the hydration through the filler effect (Lothenbach et al., 2008). The filler effect is attributed to smaller size particles filling in the spacing around the larger size or more coarse particles. This study attempts to solely view the influence of limestone powder in high volume replacement systems by eliminating the filler effect. This is accomplished by matching the particle size distribution of the cement that is being replaced by that of a blended limestone powder.

2.4. Chloride Ion Transport

Understanding the movement of ions in a porous media is crucial to determination of cement pastes with optimal durability characteristics and to understand and develop methodologies for limiting ion transport. The durability of reinforced concrete structures that are in areas prone to chloride ion ingress is of great importance (FHWA, 2002). Before steel begins to corrode there must be a certain level of chlorides present in the concrete (Xu, Jiang, & Wang, 2009). It takes years to simulate the penetration of chloride ions in a laboratory which is why equation's and models to predict the diffusion have been developed in order to accelerate the process (Lu, 1997; Stanish, Hooton, & Thomas, 2004; Streicher & Alexander, 1995; Tang, 1999; Tong & Gjørv, 2001). These accelerated tests

describe diffusion as the movement of ions subjected to a concentration gradient or chemical potential.

The most common form of measuring diffusion is through an electric potential. Researchers have previously defined the theory for the transport of chloride ions in which two driving forces: diffusion and migration are described (Streicher & Alexander, 1995; Tang, 1999).

Diffusion and migration of the ionic movement under an externally applied electric field can best be described by:

$$J_T = J_M + J_D \tag{2.4-1}$$

Where J_T is the total flux, J_M is the flux occurring from migration, and J_D is the flux occurring from diffusion.

Under steady-state conditions where the concentration of the ionic species is assumed to be infinite we can use Fick's first law to describe the flux due to diffusion:

$$\mathrm{J_D} = -\mathrm{D}\frac{\partial \mathrm{C}}{\partial \mathrm{x}} \tag{2.4-2}$$

Where D is the chloride diffusion coefficient for the given concrete, C is the chloride concentration, and x is the position.

The flux due to migration can be described using the Nernst-Plank relationship (Lu, 1997):

$$\mathrm{J_M} = \frac{\mathrm{zFD}}{\mathrm{RT}}\mathrm{C}\frac{\mathrm{U}}{\mathrm{L}} \tag{2.4-3}$$

Where z is the valence of the chloride ion, F is the Faraday constant, U is the absolute voltage, R is the universal gas constant, T is the temperature, L is the length of the specimen, and other variables as defined previously.

The equation for the total flux with the substituted terms for diffusion (2.4-2) and migration (2.4-3) is:

$$J_T = -D\frac{\partial C}{\partial x} + \frac{zFD}{RT}C\frac{U}{L} \tag{2.4-4}$$

Assuming a constant surface concentration and an infinite thickness boundary condition the non-steady-state solution to Equation 2.4-4 is:

$$C(x,t) = \frac{C_0}{2}\left(e^{\alpha x}\mathrm{erfc}\left(\frac{x+\alpha Dt}{2\sqrt{Dt}}\right) + \mathrm{erfc}\left(\frac{x-\alpha Dt}{2\sqrt{Dt}}\right)\right) \tag{2.4-5}$$

Where C_0 is the surface concentration, t is the time, $\alpha=zFU/RTL$, and erfc is the complementary error function.

Diffusion in concrete occurs under three main mechanisms: 1) pressure difference 2) concentration difference 3) electrical potential. Accelerated chloride migration tests such as the rapid chloride permeability test (ASTM C 1202) and the non-steady-state migration test (NT Build 492) are used in this study to determine the chloride transport parameters of the binary and ternary blended concrete ("ASTM C1202 - 12. Standard Test Method for Electrical Indication of Concrete's Ability to Resist Chloride Ion Penetration," 2012, "NT Build 492. Concrete, Mortar and Cement-Based Repair Materials: Chloride Migration Coeffecient from Non-Steady-State Migration Experiments," 1990). Both of these tests cause the chloride ions to penetrate under an externally applied electrical field and a concentration potential. These tests were chosen over regular saturated diffusion tests

because of the shorter testing duration time and ease of use. There are a few problems associated with these accelerated test methods. The tests do not account for the influence of chloride binding, the effect of other ions that may be present, and temperature changes within the migration cell.

The durability characteristics of concretes containing limestone powder have been investigated (Cam & Neithalath, 2010; Chen et al., 2014; Githachuri & Alexander, 2013). Amongst the major factors that influence concrete durability, Cl^- induced reinforcement steel corrosion is considered most significant. Limestone addition could significantly impact Cl^- transport through concretes based on the replacement level and presence of other synergistic ingredients in the binder. For instance, the reduction in Cl^- binding capacity of the reaction products in binders containing limestone (Ipavec, Vuk, Gabrovšek, & Kaučič, 2013) and the associated effects of dilution can adversely influence the transport parameters whereas the synergistic use of limestone with aluminous replacement materials can result in improved transport parameters (Kemal Celik, Meral, Mancio, Mehta, & Monteiro, n.d.; Ghrici et al., 2007). This study will evaluate the Cl^- transport performance of binary and ternary blend concretes containing limestone powder exposed to electrically accelerated/induced Cl^- migration to understand and quantify Cl^- transport.

2.5. Fracture Mechanics

The fracture response for the high volume replacement mortars used in this study have been characterized using the two-parameter fracture model (Bažant, 2002; Jenq & Shah, 1985). Three-point bend test on notched beams were used to determine the material fracture parameters fracture toughness (K_{IC}) and critical crack tip opening displacement ($CTOD_c$). The fracture toughness also known as the critical stress intensity factor is the

limit beyond which the crack starts growing as the width of the crack increases. The critical crack tip opening displacement is a measure of the materials ductility and is defined as the limit beyond which unstable crack propagation occurs.

The benefit of using the two parameter fracture model is that the fracture parameters are size independent and can be calculated for any proposed geometry (Jenq & Shah, 1985). The equations used for determination of the fracture parameters are:

(i) The elastic modulus (E) is given as: $E = \frac{6Sa_0V(a_0/d)}{c_i bd^2}$ (2.5-1)

Here, S is the span of the beam; C_i is the initial compliance, b and d are specimen breadth and depth respectively. $V(a_0/d)$ is the geometric correction factor.

(ii) The critical crack length a_c is obtained from the E value (2.5-1) and unloading compliance. Since $V(a_c/d)$ is also a function of a_c the equation is solved using a suitable solver function to obtain the value of a_c.

(iii) The critical stress intensity factor (K_{IC}) is obtained as:

$$K_{IC} = \frac{3(P_{\max} + 0.5W)S\sqrt{\pi a_c}\, g_1(a_c/d)}{2bd^2} \quad (2.5\text{-}2)$$

Where $P_{\max}$ is the maximum load, W is the self-weight of the beam and $g_1(a_c/d)$ is the geometric correction factor.

(iv) The critical crack tip opening displacement ($CTOD_C$) is determined as:

$$CTOD_C = \frac{6P_{\max} S a_c V_1(a_c/d)}{Ebd^2}[(1-\beta)^2 + (1.081 - 1.149 a_c/d)(\beta - \beta^2)]^{0.5} \qquad (2.5\text{-}3)$$

Where $\beta = a_0 / a_c$

3. MATERIALS, MIXTURE PROPORTIONS, AND TEST METHODS

3.1. Materials

A type I/II ordinary portland cement (OPC) conforming to ASTM C 150 ("ASTM C150 / C150M - 12. Standard Specification for Portland Cement," 2012), metakaolin (MK) and a Class F fly ash (FA) conforming to ASTM C 618 ("ASTM C618-12a. Standard Specification for Coal Fly Ash and Raw or Calcined Natural Pozzolan for Use in Concrete," 2012), and a limestone powder conforming to ASTM C 568 ("ASTM C568 / C568 - 10. Standard Specification for Limestone Dimension Stone," 2010) were used in this study. The limestone powder used in this study for cement replacement was a blend of two different median particle size limestone's, 3μm and 10μm, to match the particle size distribution of the OPC. The particle size distributions of the cement, metakaolin, fly ash, limestone powder, and composite limestone powder are shown in Figure 1. The physical characteristics and chemical composition of these materials are shown in Table 1.

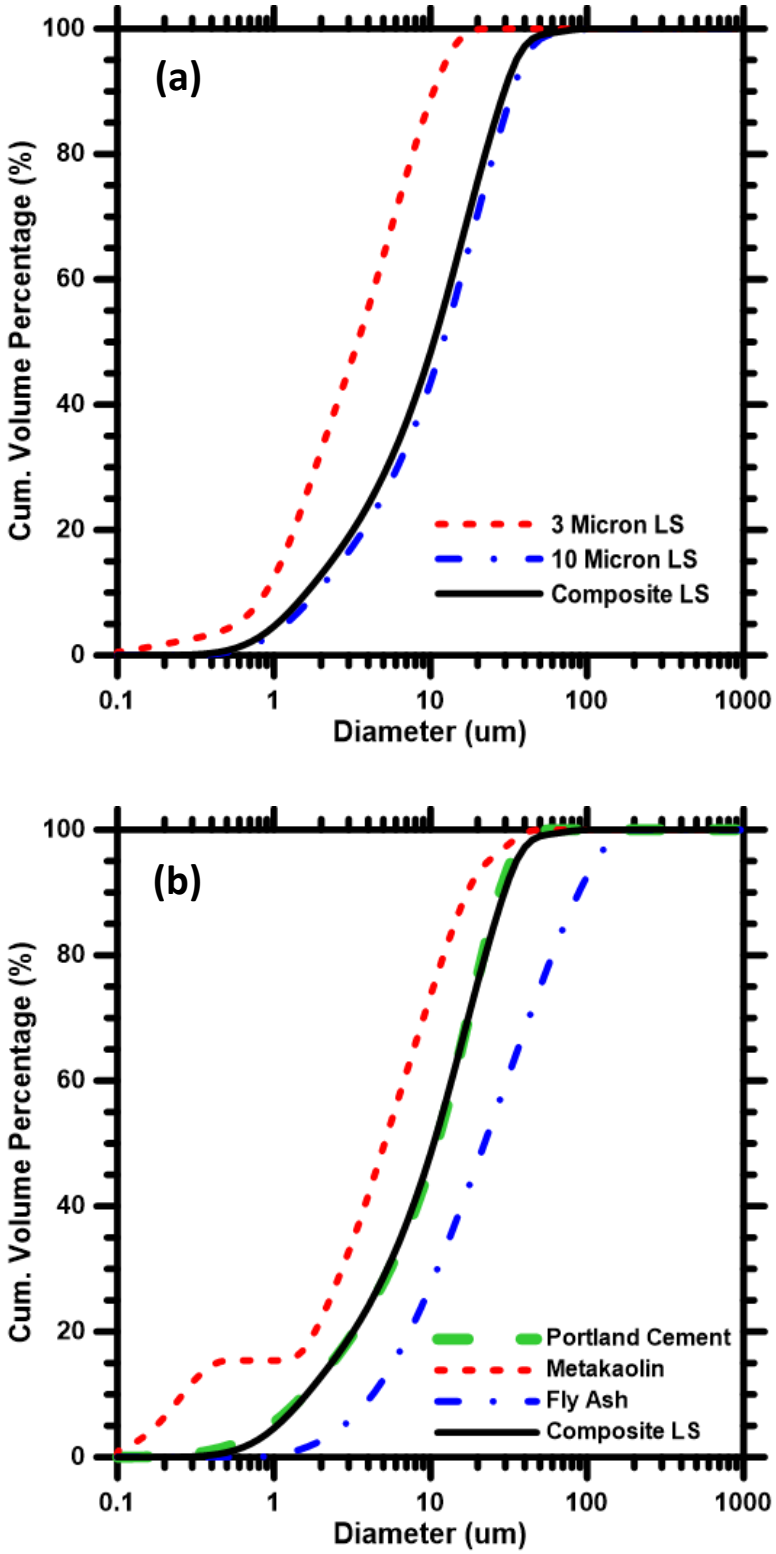

Figure 1: Particle size distribution of: (a) composite limestone powder and (b) cement, metakaolin, fly ash, and composite limestone

Table 1: Chemical composition of the component materials

Component (%)	Cement	Metakaolin	Fly ash
SiO_2	21.0	51.7	58.4
Al_2O_3	3.61	43.2	23.8
Fe_2O_3	3.47	0.5	4.19
CaO	63.0	--	7.32
MgO	3.26	--	1.11
SO_3	3.04	--	0.44
Na_2O	0.16	--	1.43
K_2O	0.36	--	1.02
LOI	2.13	0.16	0.50
D_{50} (µm)	10.5	5.1	22.5

3.2. Particle Size Determination

The limestone sizes of 3µm and 10µm were chosen from a total of four different median particle size limestone's (0.7, 3, 10, and 15µm). Using the provided sizes, a limestone was produced which was a composite of the selected limestone to minimize the squared error between the distribution of the composite limestone and the distribution of the OPC. The resultant least square optimized composite limestone was composed of 1.87% 3µm and 98.13% 10µm, by mass and contained a median particle size of 10.5 µm.

3.3. Mixture Proportions

For this study a total of ten mixtures were proportioned and evaluated with a volumetric water-to-powder ratio, $(w/p)_v$, of 1.26 (corresponding to a mass-based w/p of approximately 0.40). Mortar mixes consisting of cubes (50x50x50 mm) and beams (330x76x25 mm) were prepared for uniaxial compression and three-point bending tests, respectively ("ASTM C109 / C109M - 13. Standard Test Method for Compressive Strength of Hydraulic Cement Mortars (Using 2-in. or 50-mm Cube Specimens)," 2013, "ASTM C1609 / C1609 - 12. Standard Test Method for Flexural Performance of Fiber-Reinforced Concrete (Using Beam With Third-Point Loading)," 2012, "ASTM C192 / C192M - 13a. Standard Practice for Making and Curing Concrete Test Specimens in the Laboratory," 2013, "ASTM C78 / C78M - 10e1. Standard Test Method for Flexural Strength of Concrete (Using Simple Beam With Third-Point Loading)," 2010). Concrete mixes were prepared for uniaxial compression using 3x6 inch sized cylinders and chloride ion transport tests which utilized 4x8 inch sized cylinders. The OPC was replaced by volume percentage levels of 20% and 35%, with the binary and ternary blends containing replacement levels between 10-35% for LS, 10-35% for FA, and 10% for MK. The replacement volume by MK was limited to 10% to maintain concrete workability which is found to decrease due to the smaller particle sizes and higher surface area for MK that affects dispersion (Cassagnabère, Diederich, Mouret, Escadeillas, & Lachemi, 2013; Madandoust & Mousavi, 2012; Paiva et al., 2012). The workability for the concrete mixes was controlled using MasterGlenium® 7500, a polycarboxalate based high range water reducer (at 4% by mass of powder) conforming to ASTM C494 ("ASTM C494 / C494M - 13. Standard Specification for Chemical Admixtures for Concrete," 2013, p. 494). The mortar mixes

were proportioned using a locally available 30 grit sand at a volume fraction of 50%, and the concrete was proportioned using a total aggregate volume fraction of 70%. The ratio of fine aggregate to coarse aggregate is 0.6 and the maximum coarse aggregate size is 12.7 mm. The mixture proportions in Table 2 are for 1 m^3 of concrete (Conc.) and mortar (Mor.). The powders for each mix were dry blended for 3-5 minutes to ensure adequate distribution of replacement materials and to ensure consistency in the binary and ternary blends. All mixing was done in accordance with ASTM standards ("ASTM C150 / C150M - 12. Standard Specification for Portland Cement," 2012, "ASTM C1714 / C1714M - 13a. Standard Specification for Preblended Dry Mortar Mix for Unit Masonry," 2013, "ASTM C192 / C192M - 13a. Standard Practice for Making and Curing Concrete Test Specimens in the Laboratory," 2013, "ASTM C305 - 13. Standard Practice for Mechanical Mixing of Hydraulic Cement Pastes and Mortars of Plastic Consistency," 2013).

Table 2: Mixture proportions

Mixture	Cement (kg)		Limestone (kg)		Fly ash (kg)		Metakaolin (kg)		Coarse agg. (kg)		Fine agg. (kg)	
	Conc.	Mor.	Conc.	Mor.	Conc.	Mor.	Conc.	Mor.	Conc.	Mor.	Conc.	Mor.
Plain	480	1110	0	0	0	0	0	0	1066	0	661	846
LS 20	395	900	85	193	0	0	0	0	1065	0	660	857
FA 20	399	905	0	0	80	182	0	0	1065	0	660	862
LS 10 FA 10	397	904	43	97	40	91	0	0	1065	0	660	861
LS 10 MK 10	398	904	43	97	0	0	38	86	1063	0	659	861
LS 35	327	740	151	342	0	0	0	0	1061	0	658	867
FA 35	333	745	0	0	145	323	0	0	1061	0	658	873
LS 10 FA 25	331	743	44	98	103	230	0	0	1060	0	657	871
LS 20 FA 15	330	742	87	196	61	138	0	0	1062	0	659	870
LS 25 MK 10	330	742	109	245	0	0	39	87	1060	0	657	870

3.4. Moist Curing

The concretes and mortar specimens were subjected to moist curing at 23±2 ºC at a relative humidity > 95% after 24 hours of demolding. Samples were loosely covered in plastic for the first 24 hours to prevent water ponding on the sample in the fog chamber. Samples were demolded after 24 hours and cured uncovered in the fog chamber until the desired testing age.

3.5. Reaction Product and Pore Structure Analysis

The following test methods for determining and evaluating the reaction products were all done on representative paste samples using the same mixes from Table 2 cured under sealed conditions until desired testing age. These analyses were completed at ages of 28 and 56 days.

3.5.1. Thermogravimetric Analysis

Simultaneous thermal analysis (thermogravimetric analysis (TGA) and differential thermal analysis (DTA)) was performed to determine the hydration products, calcium hydroxide (CH) contents, and calcium carbonate ($CaCO_3$) contents of each binary and ternary mixture. The tests were performed in a nitrogen environment, with a nitrogen gas flow rate set to 20 ml/s. The samples were heated from ambient temperature to 950 ºC at a rate of 15 ºC/min. The mass loss recorded over this range was used for determination of the above listed products. Calcium hydroxide content is determined from the stoichiometric relationship related to dehydroxilization, which typically occurs between 410 and 520 °C (Dweck, Buchler, Coelho, & Cartledge, 2000). The relevant stoichiometric relationship relates the hydroxide mass loss to the overall mass of calcium hydroxide. Similarly, the

calcium carbonate content is determined from the mass loss associated with the decarbonation of calcium carbonate, which typically occurs between 650 and 850 °C (Dweck et al., 2000). The stoichiometric relationship associated with the mass loss of carbon dioxide over this range is used to determine the calcium carbonate present in the sample. The decarbonation and dehydroxilization ranges were determined by the initiation and termination of the peaks in the heat flow curves associated with these processes. The non-evaporable water content (w_n) was calculated as the difference between the mass measurements at 1000 ºC and 105 ºC, normalized by the mass at 105 ºC, and corrected for the loss on ignition (LOI) of the cement powder (based on its mass fraction of cement in the paste, where the loss on ignition was provided by the cement supplier) and the mass loss associated with calcium carbonate decarbonation.

3.5.2. Mercury Intrusion Porosimetry

The porosities of the binary and ternary pastes were determined using mercury intrusion porosimetry (MIP) at an age of 28 days. Samples were pre-treated using an oven drying methodology, wherein the samples were placed in an oven at 60 ºC for 2 hours. The MIP used is a Quantachrome Instruments Pore Master 60 porosimeter that can evaluate a minimum pore diameter of 0.003 μm and a maximum pressure of 414 MPa. The contact angle and surface tension values used were 117º and 0.485 N/m respectively, as these values are found to be typical for oven dried samples in the literature (Liabastre & Orr, 1978; D. Shi & Winslow, 1985). The porosity of the cement paste was determined as the total volume of mercury intruded divided by the volume of the sample, where the volume of the sample was determined using a sample density of 2.00 g/cc. The resultant porosity of the concrete was determined assuming the porosity of aggregates is effectively zero,

allowing for volumetric averaging to be used to determine the porosity of the resultant concrete. The pore diameters are evaluated using the Washburn equation (Washburn, 1921):

$$P = \frac{4\gamma Cos\theta}{D} \tag{3.5-1}$$

Where P is the pressure applied to the sample in MPa, γ is the surface tension of mercury, θ is the mercury contact angle, and D is the diameter of the pore. It should be noted that MIP does have its disadvantages such as the ink-bottle effect which describes the pores that are not connected to the surface directly or through larger sized pores (Moro & Böhni, 2002), MIP cannot detect isolated pores and can potentially collapse small pores or break through to isolated pores (Cook & Hover, 1999), and various preparation drying methods which influence the geometry and surface roughness of the pores (Abell, Willis, & Lange, 1999; Gallé, 2001).

Figure 2: Quantachrome PoreMaster mercury intrusion porosimetry

3.6. Scanning Electron Microscopy

Microstructural images of the samples used in this study were obtained using a Philips XL30 Field Emission Environmental scanning electron microscope (FESEM). Rectangular sections (approximately 10mm x 10mm x 5mm) were cut from the core of the paste samples using a carbide blade saw. After cutting, the samples were grinded and polished using the following procedure to achieve a representative smooth surface required for FESEM investigation. The samples were prepared using MetPrep 3^{TM} grinder/polisher with power head. 600 and 800 Grit Silicon Carbide (SiC) abrasive discs were used to remove surface striations deformations caused by the cutting of the rectangular sections. Removal of surface striations caused by grinding was accomplished by using 3 µm and 1 µm diamond suspensions for polishing. Final polishing was done with 0.04 µm colloidal silica suspension. After each grinding and polishing step the sample as well as the sample holder were cleaned using organic soap and dried using compressed air spray to prevent any cross contamination between samples. The samples were observed under an optical

microscope periodically to observe the progression of the polishing. The rotational speed varied between 150-300 RPM's for the sample holder and platen containing the grinding paper. The force from the grinder/polisher varied between 25-30 N; and the duration of each polishing step was about 3 minutes. The completed polished sample was placed in FESEM to perform the investigation.

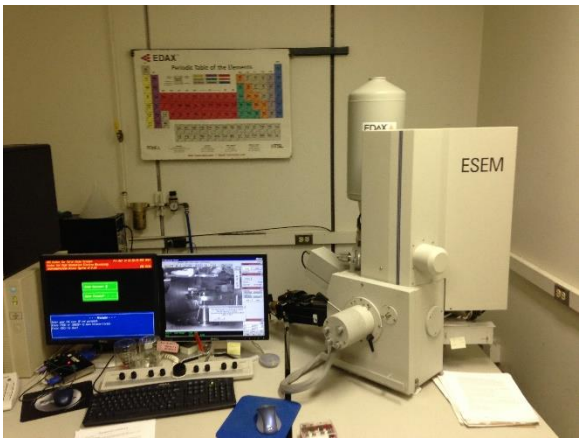

Figure 3: SEM experimental set-up

3.7. Electrical Impedance Spectroscopy

Electrical impedance spectroscopy (EIS) was performed on samples to measure the bulk resistances (R_b) before and after the NSSM test was performed. The EIS spectra were obtained using a Solarton^{TM} 1260 gain-phase analyzer. A 250 mV AC signal was employed at a frequency range of 1 Hz – 10 MHz with 10 measurements per decade. The measured impedance is represented with a Nyquist plot, which is a plot of the real versus imaginary impedance. There are two distinct figures in these plots, a bulk arc and an electrode arc. The point at which bulk arc and electrode arc meet on the real impedance axis is denoted as the bulk resistance. The effective conductivity (σ_{eff}) of the system is related to the bulk resistance through the relationship:

$$\sigma_{eff} = \frac{L}{R_b A} \quad (3.7\text{-}1)$$

Where A is the cross-sectional area (7854 mm^2) of the specimens and L is the length (50 mm).

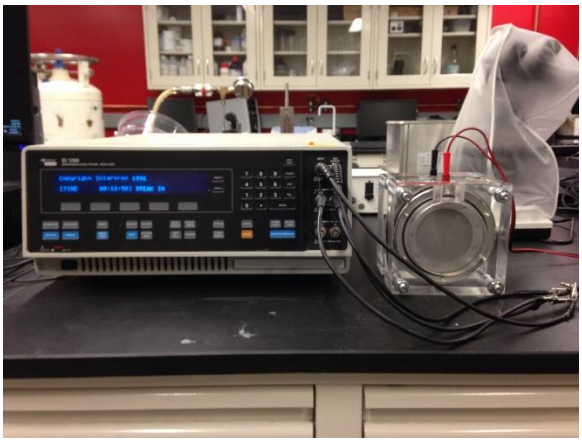

Figure 4: EIS experimental set-up

3.8. Chloride Transport

3.8.1. Sample Pre-conditioning

For both of NSSM and RCP tests, 50mm thick slices were cut from the cylindrical samples cured for 28 and 56 days as described above. Two samples corresponding to the same mix obtained from different cylinders were used for the transport tests. The average values from those two cylinders are the reported values expressed from the RCP and NSSM test throughout this study. The pre-conditioning of the sample consists of several steps as outlined below. All of the pre-conditioning steps took place at a laboratory temperature of 23±2°C. The sample is first removed from the curing chamber and air dried for one hour. After an hour, the sample is immediately placed in a vacuum desiccator for 3 hours maintaining a pressure at 1-5 kPa. After 3 hours in the vacuum desiccator, de-ionized water

or saturated calcium hydroxide for RCP or NSSM tests respectively are placed in the desiccator and the vacuum is drawn for an additional hour. After one hour in the vacuum desiccator with the selected solution, the vacuum pump is shut off, air is slowly allowed to return to the desiccator. After air has returned to the desiccator, the samples are soaked, fully submerged in the specified solution, for a period of 18±2 hours. The experimental set-up for the RCP and NSSM test is a Germann Instruments PROOVE'it Rapid Chloride Permeability Test System shown in Figure 5(b).

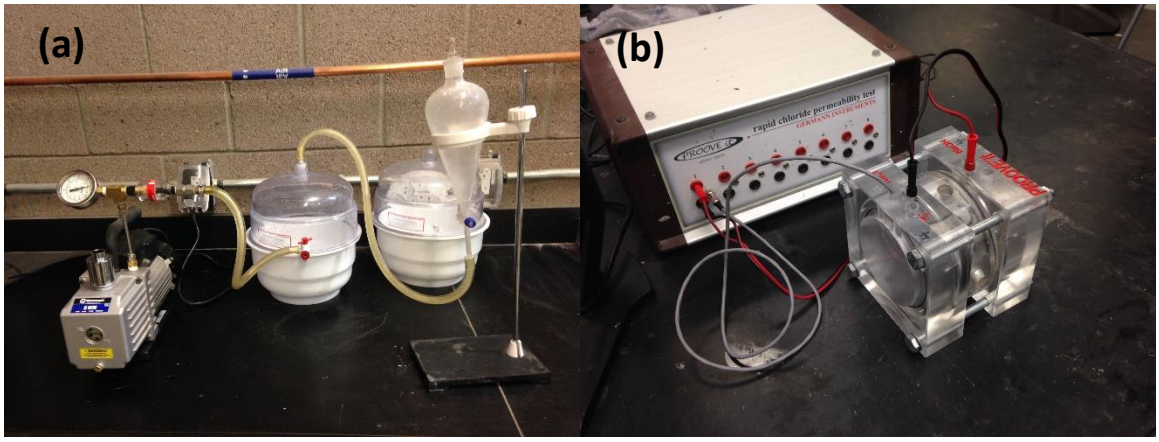

Figure 5: Experimental set-up for: (a) vacuum saturation apparatus and (b) NSSM and RCP

3.8.2. Rapid Chloride Permeability (RCP) Test

The RCP test was performed in accordance with ASTM C 1202 ("ASTM C1202 - 12. Standard Test Method for Electrical Indication of Concrete's Ability to Resist Chloride Ion Penetration," 2012, p. 12). This test determines the resistance to chloride penetration through the electrical conductance of the concrete when subjected to an externally applied potential of 60V. The electric current is monitored for a total duration of 6 hours and the total charge passed (coulombs) is expressed as the final result. The migration cell shown in Figure 5(b) uses a 3% NaCl solution in the catholyte compartment and a 0.3 N NaOH

solution in the anolyte compartment during the RCP test. During the RCP test the temperature and current is being monitored and recorded by the system every five minutes and at the end of the test the total charge passed is displayed. This total charged passed is result used for comparison in the RCP tests.

3.8.3. Non-Steady-State Migration (NSSM) Test

The NSSM test was performed in accordance with the Nordtest method (NT BUILD 492) ("NT Build 492. Concrete, Mortar and Cement-Based Repair Materials: Chloride Migration Coeffecient from Non-Steady-State Migration Experiments," 1990). This test also determines the resistance of chloride penetration through the measurement of the penetration depth and calculation of the migration coefficient. The NSSM test differs from the RCP test in several aspects: (i) the test is appreciably longer in duration (24 hours) and (ii) due to this longer duration, the externally applied voltage used is determined from the initial current in the specimen when a 30V electric potential is applied. After completion of the test the specimens are split axially (along the z-axis of the sample) and a 0.1 N silver nitrate solution is sprayed on the split surfaces. After a few minutes a visible white silver chloride precipitates on the surface and 5-7 measurements are taken representing the chloride penetration depth. An example of the white silver chloride penetration profile is shown in Figure 6. The average value of the penetration depth (x_d) as determined as the mean of the 5-7 measurements per sample is used to calculate the NSSM migration coefficient, $D_{nssm}\left(\frac{m^2}{s}\right)$, given as:

$$D_{nssm} = \frac{RT}{zFE}\frac{x_d - \alpha\sqrt{x_d}}{t} \quad (3.8\text{-}1)$$

Where

$$E = \frac{U-2}{L} \text{ and } \alpha = 2\sqrt{\frac{RT}{zFE}}\,\text{erf}^{-1}\left(1 - \frac{2C_d}{C_0}\right) \quad (3.8\text{-}2)$$

U is the absolute voltage, L is the specimen thickness, R is the molar gas constant (8.314 J/(K mol)), z is the absolute value of ion valence (1, for chloride ions), F is the Faraday constant (96,485 J/(V mol)), T is the average of the initial and final temperatures in the anolyte solution (K), t is the test duration (s), C_d is the chloride concentration that causes precipitation of silver chloride ($C_d \approx 0.07$ N for plain concrete and also for the binary and ternary concretes because the changes in C_d do not influence the NSSM migration coefficient to a noticeable degree (J. Jain & Neithalath, 2011)), and C_0 is the chloride concentration in the catholyte solution. The migration cell shown in Figure 5(b) uses a 2 N (10%) NaCl solution in the catholyte compartment and a 0.3 N NaOH solution in the anolyte compartment during the NSSM test.

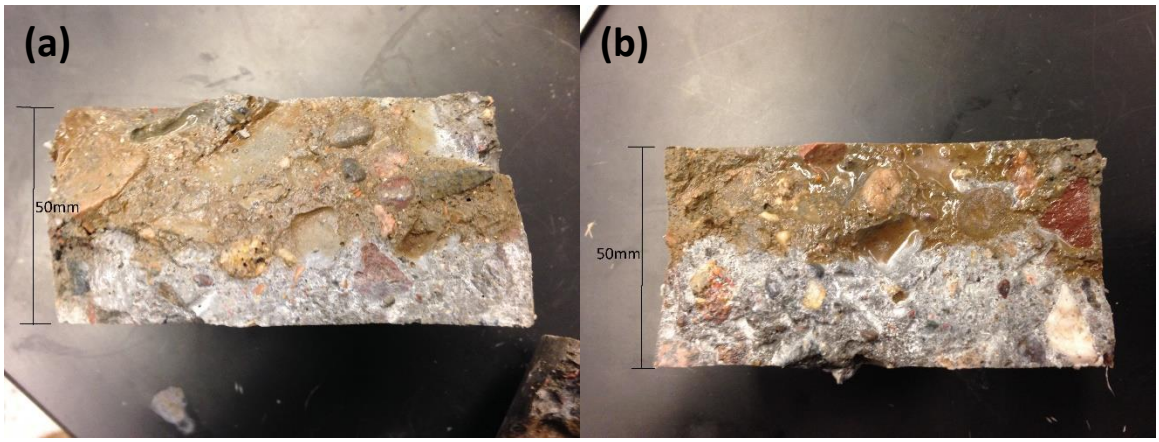

Figure 6: Chloride penetration profile for: (a) 10% limestone 10% metakaolin and (b) 10% limestone 10% fly ash

3.9. Mechanical Testing

3.9.1. Determination of Compressive Strength

The compressive strength of the mortar cubes and concrete cylinders was accomplished in accordance with ASTM C109 and ASTM C39, respectively ("ASTM C109 / C109M - 13. Standard Test Method for Compressive Strength of Hydraulic Cement Mortars (Using 2-in. or 50-mm Cube Specimens)," 2013, "ASTM C39 / 39M -14. Standard Test Method for Compresive Strength of Cylindrical Concrete Specimens," 2014). For this study the cubes were tested at ages 3-56 days and the concrete was tested at ages 28 and 56 days. Later in this study a comparison is made on the size effects influencing the difference in compressive strength between the cubes and cylinders.

3.9.2. Determination of Fracture Parameters

Mentioned earlier the fracture parameters were determined using a two-parameter fracture model (Jenq & Shah, 1985). The fracture parameters of interest in this study are the critical stress intensity factor (K_{IC}) and critical crack tip opening displacement ($CTOD_c$). These parameters are calculated using three-point bending tests on notched beams. The beams have been tested in a closed loop testing machine where the crack mouth opening displacement (CMOD) was measured using a clip gauge and provides a feedback signal to the data acquisition unit. The procedure/program used for the closed loop cyclic test is shown in Table 3.

Table 3: Closed loop cyclic test program

Sl.No.	Action	Control	Rate	Limit
1	Initial loading	Load	25 lb/min	25 lb

2	Crack opening	CMOD	0.0005 in/min	0.0015 in
3	Crack closing	Load	125 lb/min	20 lb
4	Crack opening	CMOD	0.00075 in/min	0.0025 in
5	Crack closing	Load	125 lb/min	20 lb
6	Crack opening	CMOD	0.00075 in/min	0.0035 in
7	Crack closing	Load	125 lb/min	20 lb
8	Crack opening	CMOD	0.00075 in/min	0.0045 in
9	Crack closing	Load	125 lb/min	20 lb
10	Crack opening	CMOD	0.00075 in/min	0.0055 in
11	Crack closing	Load	125 lb/min	20 lb
12	Crack opening	CMOD	0.00075 in/min	0.0075 in

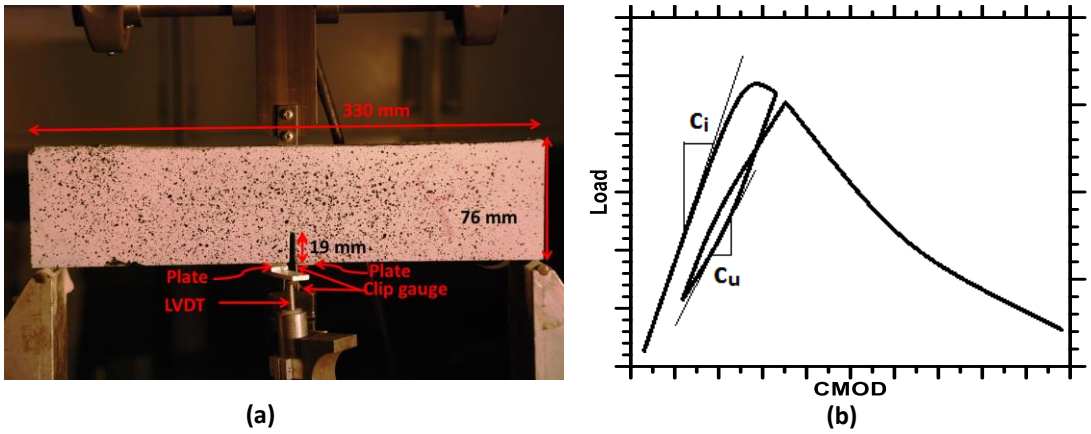

Figure 7: (a) Experimental set-up for fracture test and (b) typical load-CMOD plot with loading and unloading compliances

4. MICROSTRUCTURE AND MECHANICAL PROPERTIES

4.1. Microstructural Images

Developing an understanding of the type of microstructure present in a certain material is essential to describing the mechanical and transport behavior of these materials. In this section scanning electron images are shown in order to get a visual representation of the materials that are discussed throughout this study. Figure 8 displays the microstructural images that were obtained through a scanning electron microscope, detailed in section 3.6. The images represent the microstructure of the paste for the plain cement, binary limestone, and ternary blends of limestone and fly ash or metakaolin at an age of 28 days. Figure 8(a) and 8(b) are for the OPC, 8(c) and 8(d) are for the binary limestone at 20% replacement, 8(e) and 8(f) are for the ternary limestone-fly ash blend at 20% OPC replacement, and 8(g) and 8(h) are for the ternary metakaolin blend at 20% OPC replacement. There are two sets of images for each of the pastes, one image at 200 µm and the other at 20 µm. There is a noticeable difference between the ternary blends and that of the OPC control. The ternary blends show a much denser microstructure with more solid hydration products being formed as opposed to the more porous structure of the OPC. The binary limestone image also shows a somewhat less dense microstructure compared to the ternary blends because of the absence of an alumina source to provide additional hydration products. The following two sections will outline the type and amount reaction products in these limestone-cement systems blended with an alumina source as well as describe their pore structure.

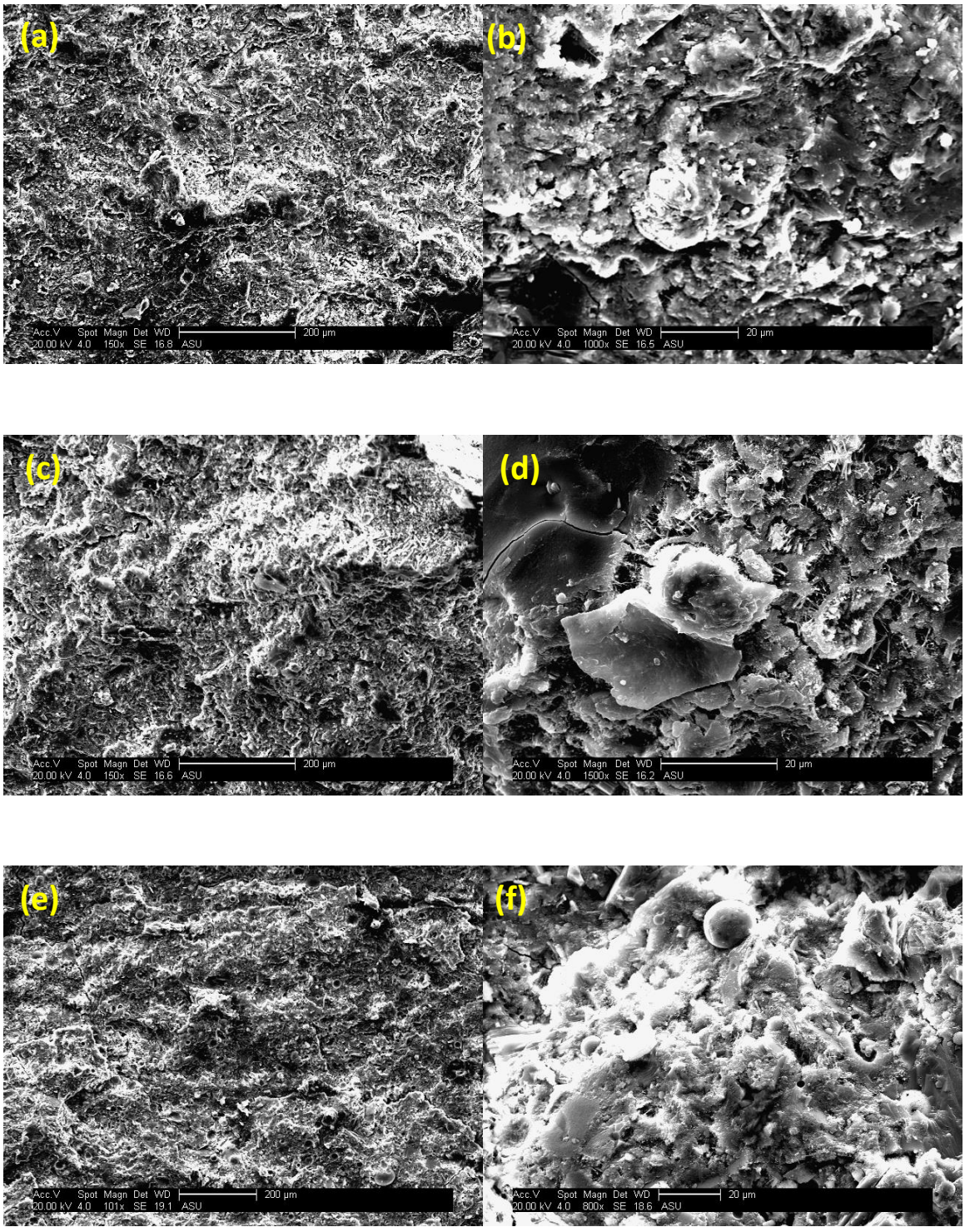
(a)
Acc.V Spot Magn Det WD
20.00 kV 4.0 150x SE 16.8 ASU
200 µm
(b)
Acc.V Spot Magn Det WD
20.00 kV 4.0 1000x SE 16.5 ASU
20 µm
(c)
Acc.V Spot Magn Det WD
20.00 kV 4.0 150x SE 16.6 ASU
200 µm
(d)
Acc.V Spot Magn Det WD
20.00 kV 4.0 1500x SE 16.2 ASU
20 µm
(e)
Acc.V Spot Magn Det WD
20.00 kV 4.0 101x SE 19.1 ASU
200 µm
(f)
Acc.V Spot Magn Det WD
20.00 kV 4.0 800x SE 18.6 ASU
20 µm

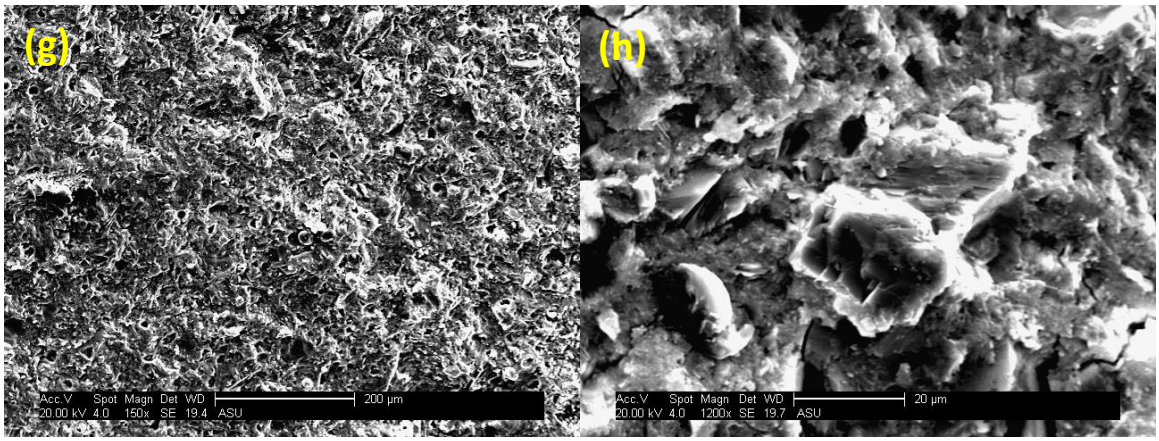

Figure 8: Microstructural images obtained from SEM for: (a, b) OPC, (c, d) 20% binary limestone, (e, f) 10% limestone 10% fly ash, (g, h) 10% limestone 10% metakaolin (28 days of hydration) at 200 µm and 20 µm

4.2. Reaction Products

The early age synergistic effects of the reaction products for binary and ternary blends containing fly ash and metakaolin in combination with limestone has been extensively reported elsewhere (Vance et al., 2013). While those studies from our research group focused on size classified limestone powder blended with OPC, this study blends limestone powders to obtain the same particle size distribution as the OPC. This helps eliminate the particle size effects in the reaction sequence and facilitates a discussion of the chemical effects of limestone in OPC systems.

This section outlines the 28 day thermal analysis of the 20% and 35% OPC replacement blends, experiments and analysis of which were completed as discussed in Section 3.5.1 and 3.5.2. Thermal analysis is important for determining the composition of these cement based systems. Calcium silicate hydrates (C-S-H) and ettringite are among the important hydration products formed in OPC. The densification of the material microstructure is highly dependent on the type and amount of these hydration products which influence the mechanical and transport properties. It has been shown that additional hydration products

such as mono/hemi-carboaluminate hydrates can form from the reaction of carbonates in limestone in the presence of an alumina (Al_2O_3) source and calcium hydroxide (De Weerdt, Haha, et al., 2011; Lothenbach et al., 2008). Since there are two types of SCM's used in this study, fly ash and metakaolin, with bulk alumina contents of 24% and 43% respectively there should be some formation of the carboaluminate phases. Figure 9 shows the heat flow curves from the thermal analysis studies. The heat flow values in this figure are normalized by the total mass of the sample at 105 °C. Noted for all mixes are three distinct peaks at sample temperatures of approximately 100, 450 and 800 °C. The first peak corresponds to the loss of evaporable water and the decomposition of both C-S-H and ettringite (De Weerdt, Kjellsen, et al., 2011; De Weerdt, Haha, et al., 2011). The second and third peaks correspond to the dehydroxilization of calcium hydroxide and the decarbonation of calcium carbonate respectively. As the heat flow curves are normalized by the total sample mass at 105 °C, one can qualitatively connect the intensity of the respective heat flow peak to the amount of that hydration product. The decomposition of C-S-H and ettringite and the loss of evaporable water is indicated by the peak at approximately 100 ºC. Figure 9(a) shows the heat flow curves for the binary limestone systems at both levels of replacement. The peak at 100 ºC is similar for the binary blends and the control OPC and the two peaks corresponding to calcium hydroxide and calcium carbonate are higher for the blended systems. In Figure 8(b), the ternary blends at 20% OPC replacement show an intense peak at 100 ºC than the control OPC. This suggests that in the presence of limestone the alumina sources are responsible for enhancing the amounts of C-S-H and/or stabilizing ettringite (Vance et al., 2013). From Figures 9(b) and 9(c), at both replacement levels in the ternary blends (20% and 35%), the blend containing metakaolin shows the highest peak at 100 ºC

and a slight peak at 180 ºC. The peak at 180 ºC corresponds to the formation of the carboaluminate phases (De Weerdt, Haha, et al., 2011; Lothenbach et al., 2008). Similarly the peak corresponding to calcium hydroxide at 450 ºC is the lowest for these two metakaolin blends. It can be inferred from these observations that the blends containing metakaolin are in fact producing more reaction products through formation of carboaluminate phases and the increased consumption of calcium hydroxide, which is an indication of its pozzolanic activity. For the binary and ternary blends of fly ash, there is a slight peak at 180 ºC indicating these blends also have some carboaluminate phases but they are not as pronounced as in the metakaolin blends. At an age of 28 days it is possible that the aluminate species in fly ash has not reacted sufficiently (attributable to the rather slow kinetics of pozzolanic reaction of fly ash) and as a result would limit the amount of reaction products formed (De Weerdt, Kjellsen, et al., 2011; De Weerdt, Haha, et al., 2011).

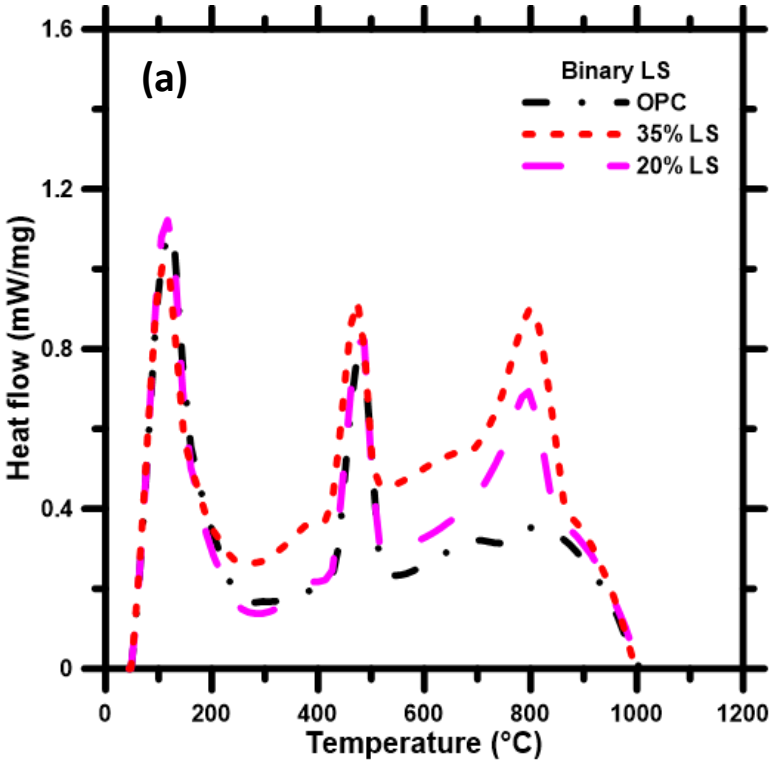

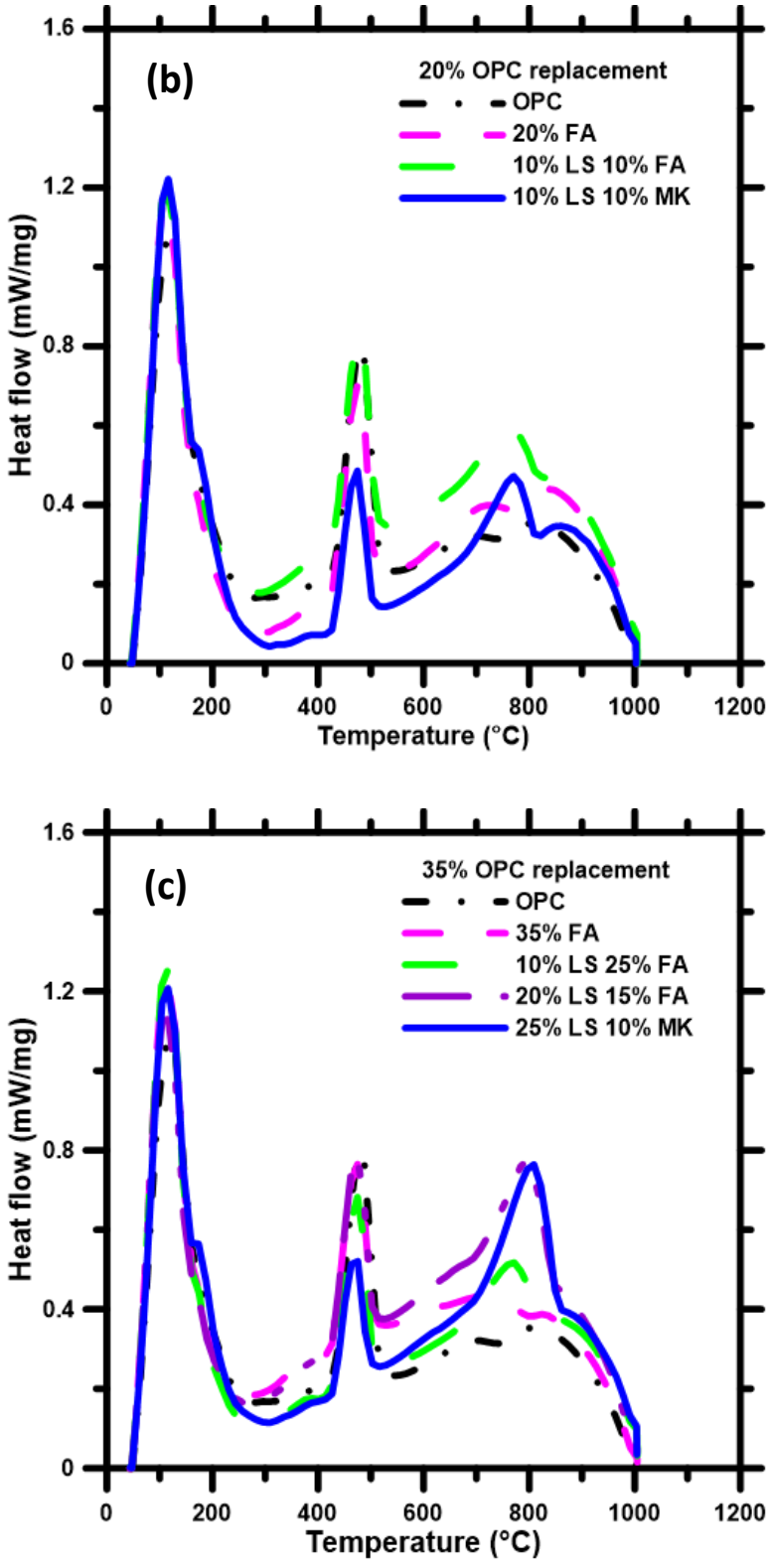

Figure 9: Heat flow curves of the limestone modified pastes at 28 days of hydration for: (a) Binary LS, (b) 20% OPC replacement, and (c) 35% OPC replacement

Figures 10(a) and 10(b) show the non-evaporable water contents (w_n) and the CH contents respectively, for the binary and ternary blends at both replacement levels (20% and 35%) at 28 days of hydration. The non-evaporable water content of a paste sample is representative of the degree to which the hydration process has progressed. It represents the amount of water that is chemically bound in C-S-H and other phases (Neithalath, Persun, & Hossain, 2009; Schwarz & Neithalath, 2008). The non-evaporable water content of a sample was determined as outlined in Section 3.5.1, where the mass of non-evaporable water was determined as the weight loss of the dried sample up to 1000°C, minus the contribution of calcium carbonate. This quantity is normalized by the dry sample weight (the weight at 105 °C), and the relevant loss on ignition is subtracted from this quantity. The weight percent of non-evaporable water in a dried sample was related to the degree of hydration of that sample as discussed in (Lam, Wong, & Poon, 2000; Zeng, Li, Fen-chong, & Dangla, 2012).

Several trends are immediately evident from Figure 10: (i) the non-evaporable water content is seen to be generally higher for the lower replacement ratio cements, with the exception of the mixes containing metakaolin, (ii) at the same replacement ratio, the inclusion of metakaolin results in a noted increase in w_n, and (iii) the inclusion of fly ash appears to have the opposite effect, as fly ash modified mixtures tend to have the lowest value of w_n amongst the pastes investigated. Higher non-evaporable water at lower replacement ratios with the inclusion of limestone is likely attributed to the low reactivity of limestone in these systems (De Weerdt, Kjellsen, et al., 2011; De Weerdt, Haha, et al., 2011; Deschner et al., 2012) as well as the relatively low pozzolanic activity of fly ash at

early ages. As the limestone content is increased, the quantity of reactive material decreases, decreasing the non-evaporable water content. Further, it is noted that inclusion of limestone on a volumetric basis results in a higher effective water-to-cement ratio. At a higher water-to-cement ratio, it is expected that the non-evaporable water content would go up (Berry, Hemmings, & Cornelius, 1990; R. F. Feldman, Carette, & Malhotra, 1990; Fraay, Bijen, & de Haan, 1989; Marsh & Day, 1988; Y. M. Zhang, Sun, & Yan, 2000), however the presence of a relatively inert filler, limestone, decreases the evaporable water content. The second effect, i.e., increasing non-evaporable water with the addition of metakaolin, is most likely related to the enhanced reactivity of metakaolin at early ages. Further, metakaolin has been shown to enhance the reactivity of limestone in portland limestone cements (Antoni et al., 2012; Madandoust & Mousavi, 2012; Perlot, Rougeau, & Dehaudt, 2013; Qian & Li, 2001).

Figure 10(b) presents the calcium hydroxide contents in these systems as a function of the mass of the hydration products. The quantity of calcium hydroxide present in a hydrated portland cement paste decreases with the formation of secondary C-S-H where calcium hydroxide combines with the siliceous components in the fly ash and metakaolin (Kar, Ray, Unnikrishnan, & Davalos, 2012). The CH content of the ternary blends containing metakaolin is found to be the lowest of all the mixtures. Normally in cement hydration, an increase in w_n generally indicates an increase in the CH content. The opposite trend demonstrated by the ternary metakaolin blends imply the formation of carboaluminate hydrates and the consumption of CH due to the pozzolanic reaction. This is evident by observing the heat flow curve of the ternary blends containing metakaolin which show the highest peak at around 100 ^{o}C (indicative of increased C-S-H), a prominent peak around

180 ºC (indicative of the formation of carboaluminate hydrate and/or ettringite stabilization), and the lowest CH peak around 475 ºC. Using reactive aluminate sources, the increased volume of reaction products compensates for the reduced cement content at higher levels of OPC replacement (by volume). The synergistic effects in the ternary blends containing limestone are attributed to: (i) the highly reactive metakaolin and fly ash that forms pozzolanic C-S-H and (ii) the carboaluminate formation through the reaction between the carbonates from the limestone powder and the aluminates from the fly ash and metakaolin. Inclusion of limestone which is finer than portland cement may increase reactivity as compared to the portland limestone binary blends presented in this work. The replacement of fine limestone by portland cement would increase the total surface area of the system, thereby decreasing the spacing between cement particles and possibly enhancing the reactivity relative to portland cement systems with coarser limestone. This aspect has been covered in detail in previous publications (V. Bonavetti et al., 2003; Lothenbach et al., 2008; Oey et al., 2013; Vance et al., 2013).

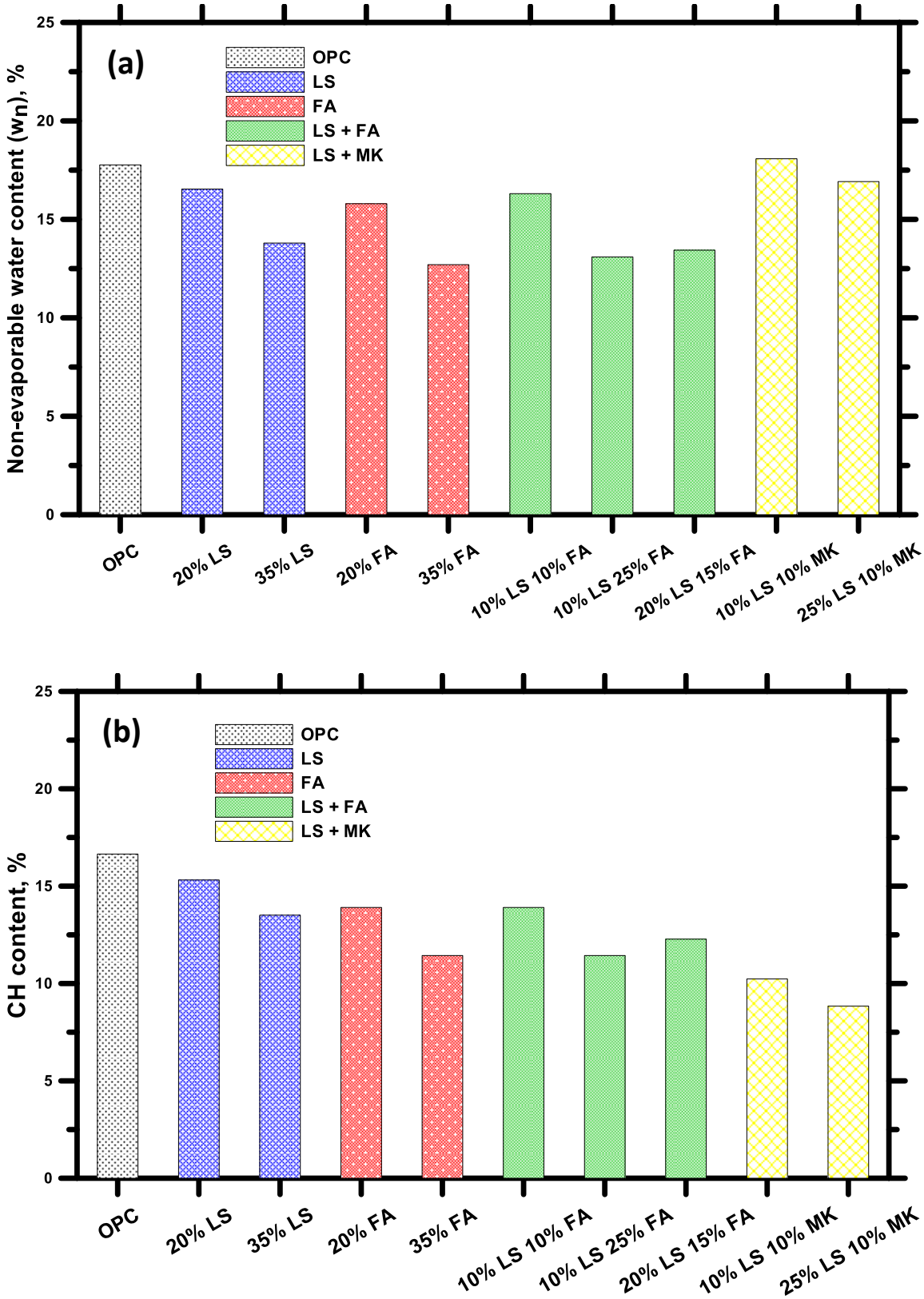

Figure 10: (a) Non-evaporable water content and (b) CH content at 28 days

Figure 11 presents the residual calcium carbonate fractions present in the sample at 28 days, normalized by the initial mass of the sample. The amount of calcium carbonate that participate in the hydration reactions are dependent on the initial amount of limestone in the mixture, its physical characteristics (size, distribution, surface characteristics), and as described above, the presence of reactive aluminous species in the system. For the ternary blends with fly ash and metakaolin at 20% OPC replacement with a limestone content of 10%, the residual calcium carbonate fractions are similar. However, increasing the amount of fly ash at the higher OPC replacement level of 35% shows that at least 2% more calcium carbonate was consumed in these mixes. This trend is not obvious in the ternary metakaolin mixes at both replacement levels. These mixes show that a similar amount of calcium carbonate was consumed and there is a threshold value at which the amount of limestone does not influence the behavior drastistically. The 35% binary limestone paste shows a residual calcium carbonate content more than double the amount consumed by the 20% binary limestone. This may be indicative of the larger amount of smaller size limestone particles (3 μm) required to match the particle size distribution of the OPC. The benefit of using smaller size particles as described earlier in this section is that they provide nucleation sites accelerating some of the hydration, and to a limited extent taking part in the hydration reaction (Vance et al., 2013).

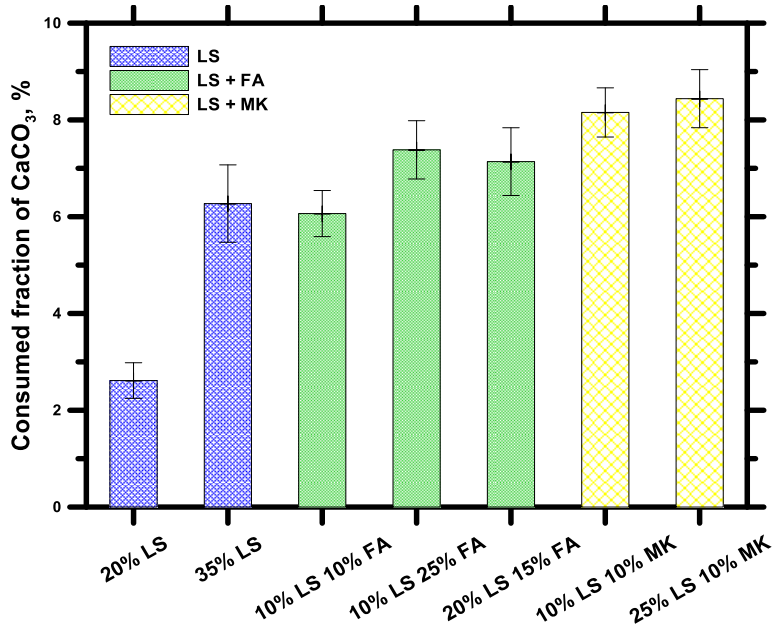

Figure 11: 28 day residual calcium carbonate fraction for binary and ternary blends containing limestone

4.3. Pore Structure

The mechanical and durability performance of cementitious materials, are highly dependent on the pore-structure of the material. The previous section explored the hydration products formed in these materials, and this section will examine the pore-structure of these materials using mercury intrusion porosimetry (MIP). This investigation was carried out using the methodology presented in Section 3.5.2. A typical pore size distribution determined using MIP is presented in Figure 12. The x-axis in Figure 12 shows the mean pore diameter which is determined by the total volume of mercury (Hg) intruded. The left y-axis in Figure 12 is the volume of mercury intruded (cm^3/g) and the right y-axis in Figure 12 is the differential curve of the volume intruded with respect to the diameter ($cm^3/g/\mu m$). As noted previously, the pore size distribution determined from MIP have been shown to be unreliable due to several key disadvantages of this method, but as a comparative method, this is a very useful microstructural tool.

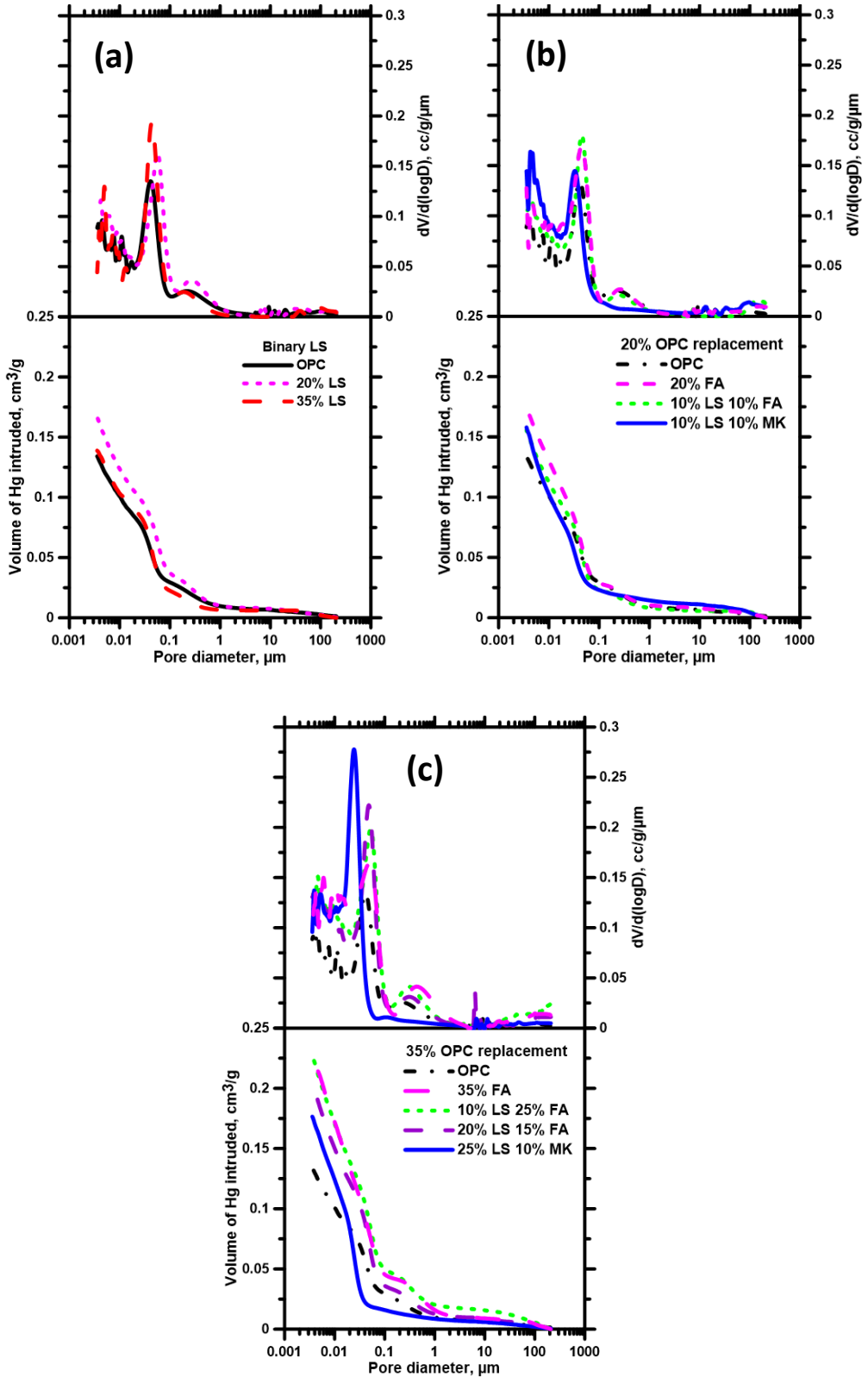

Figure 12: Total volume of Hg intruded and differential volume for: (a) binary LS, (b) 20% OPC replacement, and (c) 35% OPC replacement

Using the curves denoting the total volume of Hg intruded in Figure 12, the total porosity was determined by the procedure described in section 3.5.2 and is shown in Figure 13. All of the pastes show higher porosities than the OPC control pastes. The ternary blends containing 35% OPC replacement shows the highest porosity, as expected since the replacement materials in such high volumes are not efficient in producing hydration products as compared to OPC. As the volume of limestone is increased, the quantity of reactive material is also decreased. This results in a decrease in reaction product formation as described in the section 4.1. It is also possible that at 28 days it is still early for some of the pozzolanic reactions to occur especially in the fly ash blends. Similarly, as the particle size distributions of the replacement material are similar to that of OPC, the effect of packing is negligible, and thus there is no additional size distribution related benefits. Further contributing to this effect is the previously noted effect of volumetric replacement of cement by limestone resulting in a higher effective water-to-cement ratio by mass. A higher water-to-cement ratio results in an increase in both the porosity and the average pore diameter in the cement pastes (Atahan, Oktar, & Taşdemir, 2009; Moon, Kim, & Choi, 2006; Zeng, Li, Fen-Chong, & Dangla, 2012).

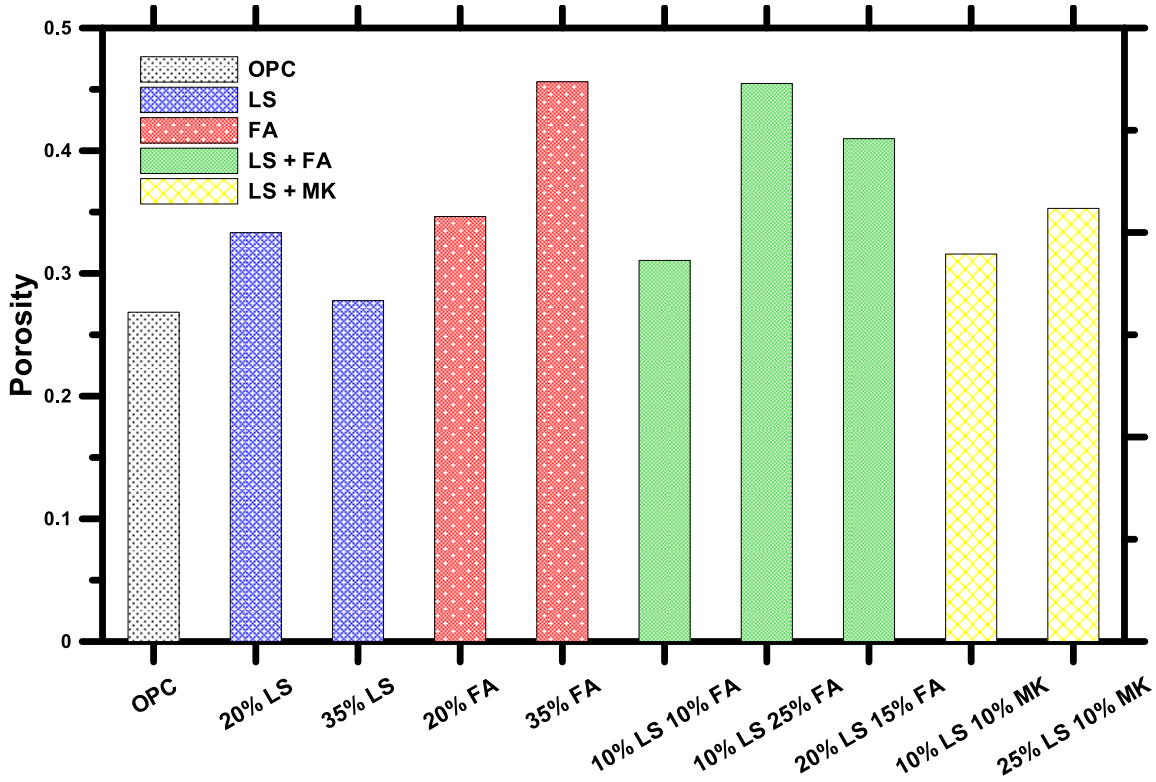

Figure 13: Porosity of the cement pastes at 20% and 35% OPC replacement (28 days)

One proposed method of comparing the pore structure of porous media and investigating the comparative differences is through the use of the average pore diameter (Moon et al., 2006). The average pore diameter is an approximate representation of the size of the pores by utilizing the total volume of mercury intruded and the total surface area of the pores. The average pore diameter,d_a, is calculated as:

$$d_a = \frac{4V}{A} \qquad (4.2\text{-}1)$$

Where V is the total volume of mercury intruded per gram of sample (cc/g), A is the total surface area of capillary pores (m^2/g) (Moon et al., 2006), where pores are assumed to be cylindrical in shape. Figure 14 shows the average pore diameter for the binary and ternary blends at 20% and 35% OPC replacement level at an age of 28 days. At both replacement

levels the porosity for the binary limestone and fly ash mixes are greater than OPC, however, by considering the total surface area within the capillary pores and using equation 4.2-1 the average pore diameters are very similar compared to the OPC control mixture. The average pore diameter provides an indication the general pore sizes present in these different blended systems. It is once again seen that the ternary limestone-metakaolin blends show the smallest average pore size which was initially eluded to in Figure 12, where the slope of the volume intruded curve for the metakaolin was noticeably lower than the other blends. It would be expected that the fly ash blends should refine the pore structure lowering the average pore diameter, except that at 28 days the pozzolanic reaction has not contributed to the refinement for reasons explained earlier in previous sections.

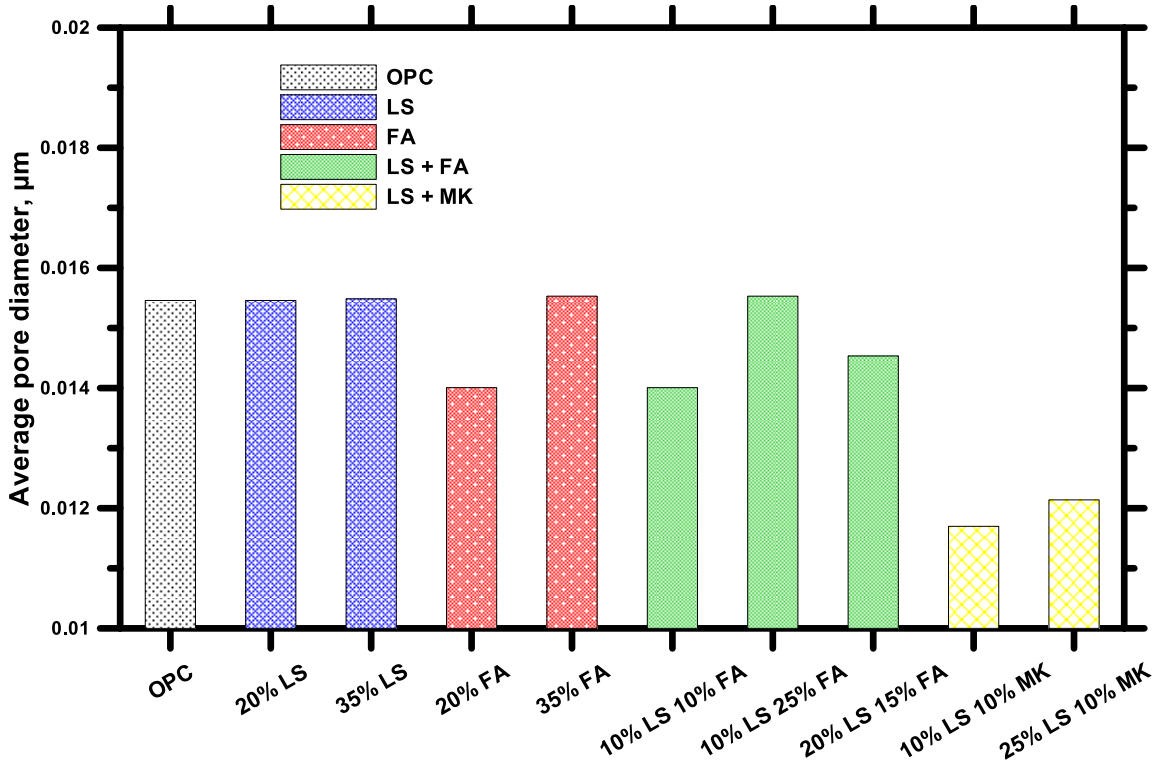

Figure 14: Average pore diameter of 20% and 35% cement pastes at 28 days of hydration

The highest volume of mercury intruded corresponds with the 35% OPC replacement pastes which indicate these samples have a higher porosity and higher surface area in the capillary pores due to a less refined pore-structure. The non-evaporable water content defined earlier is representative of the degree of hydration for these blended systems. Figure 15 shows the relationship between non-evaporable water content and the porosity. As the non-evaporable water content increases, the porosity is shown to decrease, as expected. The 35% limestone modified paste deviates from this relationship, with a lower total porosity. It is quite inconceivable that the high volume limestone incorporation would yield better properties in the absence of a reactive alumina source, and this value is considered to be an experimental anomaly. .

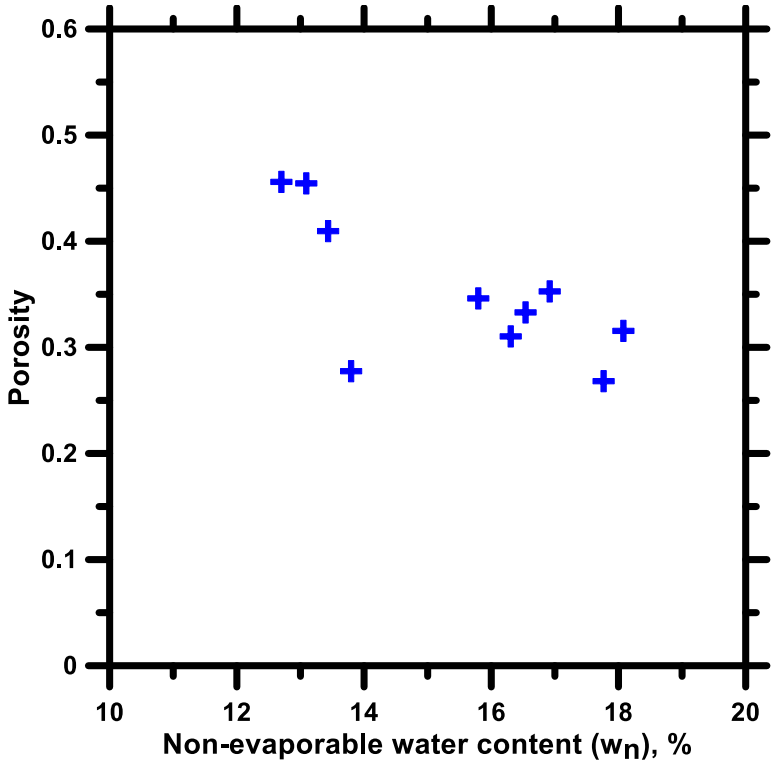

Figure 15: Non-evaporable water content and porosity comparison at 28 days

The critical pore diameter shown in Figure 16, also called the threshold or percolation pore diameter is the dominant peak on the differential volume intruded curve which was shown in Figure 12. This value represents the diameter at which the rate of volume intruded is the highest, and is thought to be representative of the pore size at which mercury percolates to the pore structure in the sample (Atahan et al., 2009; Sakai, Nakamura, & Kishi, 2014; Yu & Ye, 2013). Thus, it represents the diameter at which percolation is likely to occur, at to some extent the tortuosity of the sample, which are crucial terms in describing the transport of moisture and ionic species through the cement paste.

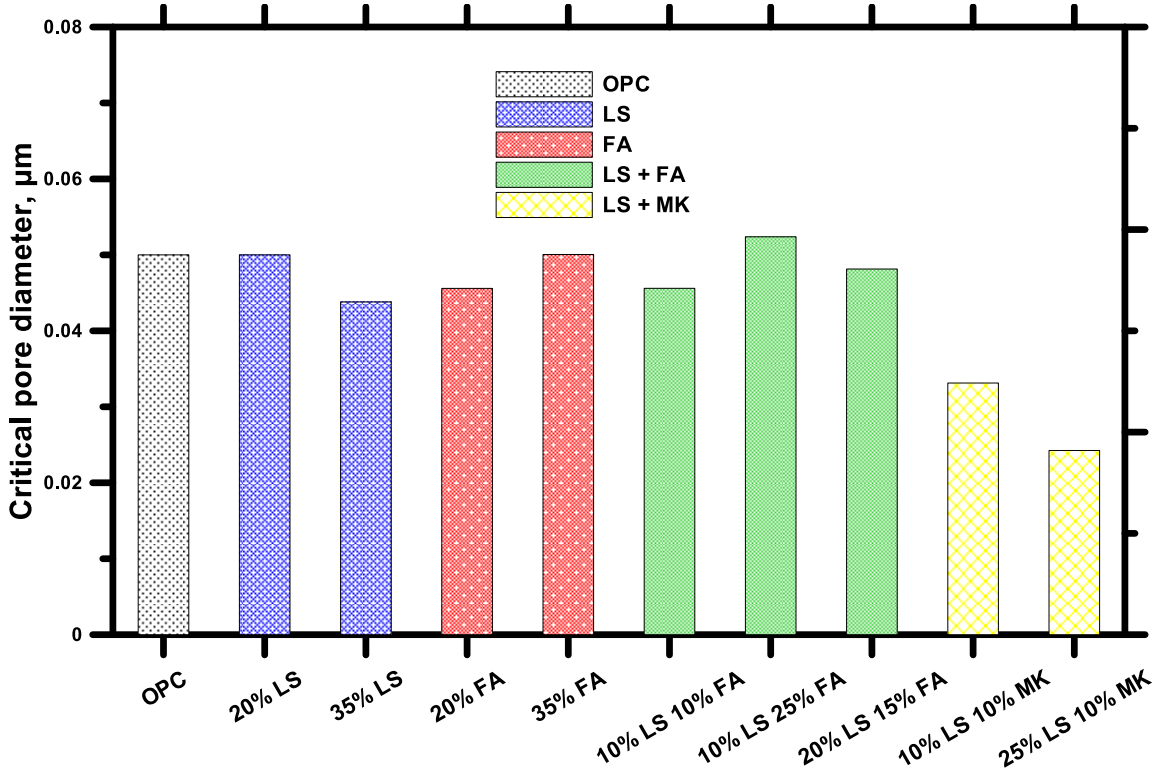

Figure 16: Critical pore diameter cement pastes for 20% and 35% OPC replacement (28 days)

It would thus be expected that there is a relationship between the critical pore diameter and the average pore diameter. There is a general trend that increasing the critical pore diameter

results in an increase in the average pore diameter as presented in Figure 17. The range of this relationship is small for the critical pore diameter (0.02-0.06 µm) and even smaller for the average pore diameter (0.012-0.016 µm) which is an indication that sizes of pores for these blended systems are similar even at large levels of OPC replacement. From Figures 14 and 16 the average and critical pore sizes are very similar to the OPC control paste with the exception of the metakaolin blends. The pore sizes for metakaolin blends are much lower than that of the OPC control because of the increased formation of hydration products and the effect of pozzolanic reaction in refining pore sizes.

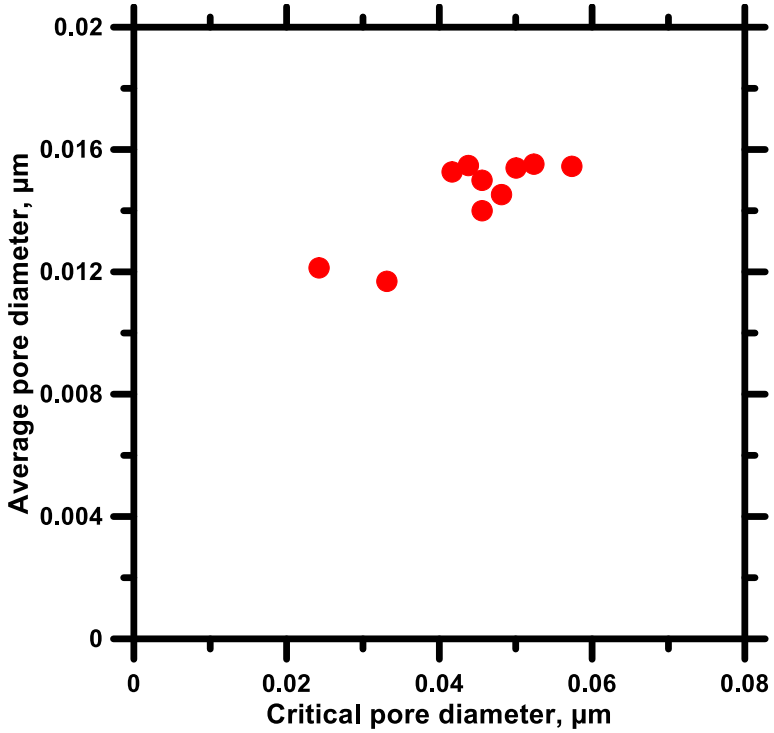

Figure 17: Critical pore diameter and average pore diameter comparison

There is good agreement between the relationship for critical pore size and the porosity of these blended systems, which is shown in Figure 18. The two values that deviate from the

observed relationship are the metakaolin blends for which the pore size is much lower, the reasons for which were described in adequate detail in the foregoing sections.

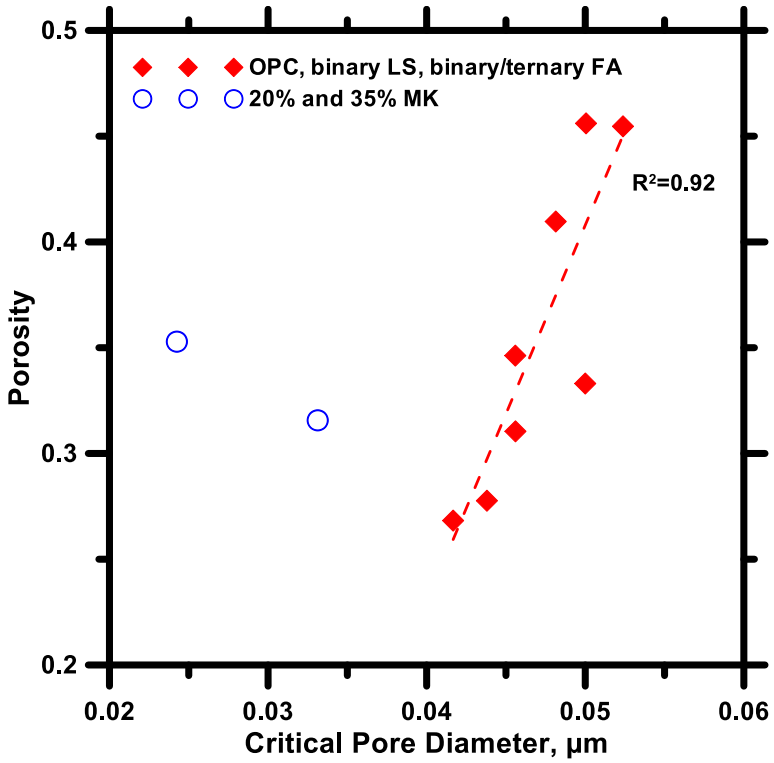

Figure 18: Relationship between critical pore diameter and porosity

4.4. Compressive Strength of Binary and Ternary Blended Mixtures

Compressive strength tests were carried out on binary and ternary blend concretes and mortars as outlined in Section 3.9.1. The results of this study are presented in Figures 19 and 20 with only the average values reported to prevent cluttering (the S.D. in these figures ranged from 1 MPa at early ages to 6 MPa at later ages). At the 20% OPC replacement level, several key results are noted: (i) the ternary blend of limestone and metakaolin is shown to have the highest compressive strengths at all ages, (ii) the binary limestone mix is seen to have a comparable strength gain at early age as indicated by the slope up to an age of 10 days and then levels off and remains relatively constant at later ages, (iii) there

does not appear to be a significant benefit of inclusion of fly ash in limestone blended cements, as noted by the comparatively low compressive strengths even at later ages, which is only marginally higher than the binary OPC-limestone blend, and (iv) in general, all the mixtures show relatively comparable compressive strengths at later ages, with the difference between the highest strength and lowest strength of only about 15%. The ternary blend containing 10% limestone and 10% metakaolin demonstrates the highest strength at all ages. This is in line with the observations made in section 4.1 and 4.2, where these mixes showed the largest amount of reaction products formed and lowest pore sizes, which has also been reported elsewhere (V. L. Bonavetti, Rahhal, & Irassar, 2001; Kadri et al., 2011; Lothenbach et al., 2008; Vance et al., 2013). The reasons for the synergistic effect of metakaolin and limestone has been described earlier. The mixture containing 20% OPC replacement by fly ash shows a strength similar to that of the control mixture at 56 days (due to the later age pozzolanic reaction of fly ash (Deschner et al., 2012)),but a lower strength at earlier ages, which is consistent with the data presented in (K. Celik et al., 2014; Kemal Celik et al., n.d.; Deschner et al., 2012). The early age strength reduction is attributed to the lower pozzolanic reactivity of fly ash at early ages, while at later ages fly ash is more reactive and the strength gain due to fly inclusion becomes significant. On the other hand, the ternary blend with fly ash and limestone shows similar strengths as the binary blend containing limestone, indicating little or no benefit from the inclusion of fly ash in this system. This behavior is attributed to higher porosities and lack of pozzolanic reaction development shown in sections 4.1 and 4.2, respectively.

Figure 19(b) shows that at 35% OPC replacement levels, all the mixtures have lower strengths at all ages than that of the control OPC mortar. Mixtures containing fly ash show

a lower strength loss compared to OPC at later ages, however there is still a 15-25% decrease in strength compared to the OPC mortar. At early ages, the blend with LS and MK is comparable in strength to the OPC mix, however at later ages this mix also shows a significantly lower strength as compared to that of the OPC system. The early age strength gain is attributed to the highly reactive metakaolin for reasons stated earlier. The 20% OPC replacement binary mixture containing limestone and the 20% OPC replacement ternary fly ash mixture has the lowest later-age strength which reinforces the idea that fly ash inclusion does not provide large benefits is limestone blends. Generally at 35% replacement, it is noted that all mixes have approximately the same strength at later ages, while there are some differences in strength gain at early age. The compressive strength results indicate that concretes with up to 20% replacement of OPC solely by limestone or in combination with other OPC replacement materials such as fly ash or metakaolin can be proportioned to display strengths within 90% of the control OPC mixture. Even at 35% replacement levels of OPC, ternary mixtures can be proportioned to display strengths within 80% of the control OPC mixture at 56 days. Other methods such as using a lower w/s can be used as a strategy to proportion comparable-strength, high-volume limestone concretes, if desired.

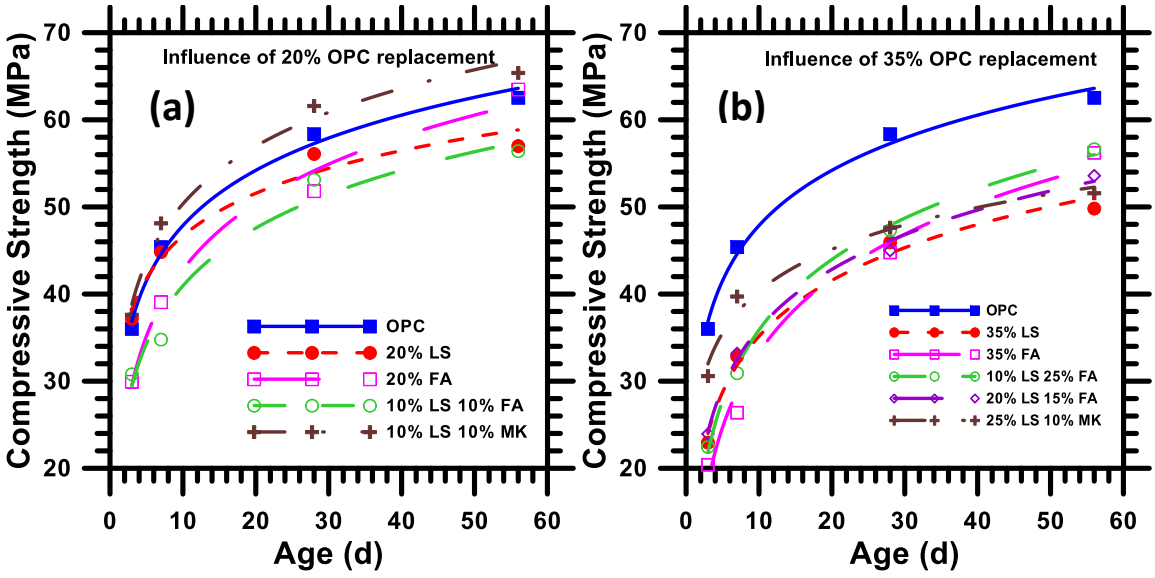

Figure 19: Compressive strength development of: (a) 20% OPC replacement and (b) 35% OPC replacement

Compressive strengths of concrete cylinder specimens were also performed using the methodology presented in Section 3.9.1. The results of this study, and the comparison of mortar and concrete strengths are presented in Figure 20. Noted from this figure is that the mortar and concretes follow the same general trend at 28 days. It is also noted that the compressive strengths of the mortars is significantly higher than that of the concretes for all samples tested. This is because the concrete mixture is more heterogeneous that the mortar. Size effects of testing samples (50 mm diameter x 50 mm diameter cubes for mortars, whereas 100 mm diameter x 200 mm high cylinders for concretes) could also have contributed to this effect.

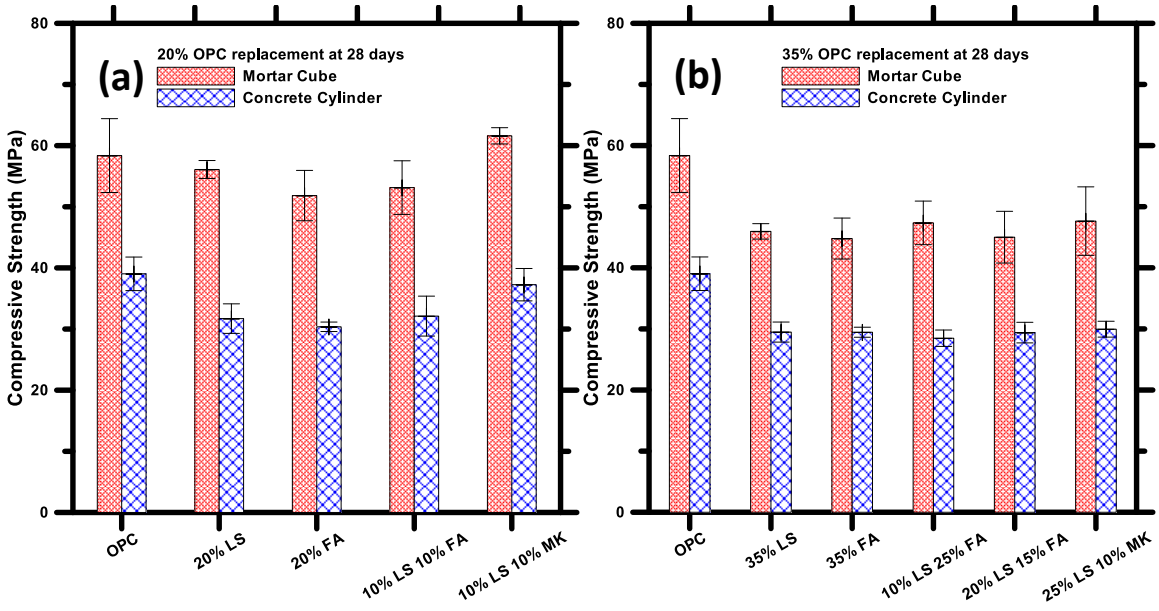

Figure 20: Compressive strength comparison at 28 days: (a) 20% OPC replacement and (b) 35% OPC replacement

4.5. Fracture Parameters

Crack mouth opening displacement (CMOD) controlled tests on notched beams were performed on ternary and binary limestone blended mortar mixtures as described in Section 3.9.2. The results of these tests that relate the load carried by the specimen to its CMOD are presented in Figure 21. The test consists of loading the specimen up to a displacement of 0.0015 inches corresponding to about 95% of the peak load, then unloading and loading over a set sequence detailed in Table 3. Figure 21 shows the representative responses for the OPC control, binary limestone, ternary fly ash and metakaolin blends at both levels of OPC replacement, 20% and 35%. Since limestone is essentially a filler in the system, there remains a substantial fraction of limestone that does not participate in the hydration reactions. The beneficial influence of limestone on the post peak behavior of the concrete is thus attributed primarily to the softer limestone particles which remain in the concrete and increase the energy-dissipation, resulting in a higher post peak response.

The peak load associated with the 20% binary limestone blend is higher than the 35% binary limestone blend and the OPC control as demonstrated in Figure 21(a). It is known that the crack growth rate is largely dependent on the loading-rate (Bažant & Gettu, 1992). The loading rate for these samples is consistent with the procedure outlined in Table 3. Therefore, the higher peak load in 20% binary limestone blends can be attributed to a change in the crack growth rate due to a few possibilities: (i) an increase in the loading rate or (ii) inelastic deformations within the fracture process zone which directly influence the growth of the crack (Bažant & Gettu, 1992) by blunting at the crack tip. Since the same cyclic program procedure was used for every sample tested the possibility of the increase in loading rate can be neglected. It is possible that at a 20% OPC replacement level, the softer particles of limestone are causing more inelastic behavior in the fracture process zone that are directly influencing the crack growth rate and ultimately the peak load. The decrease in peak load for the 35% binary limestone can be attributed to the strength-decreasing effect of the softer particles becoming more dominant at higher replacement levels.

The ternary blends at 20% OPC replacement levels show equivalent or higher peak load, improved toughness, and residual load as indicated by the higher post peak response compared to the OPC control. At the 20% replacement level, it is evident from the figures that metakaolin replacement leads to improved fracture properties. This enhanced behavior is likely attributed to the presence of a larger number of smaller pores in the metakaolin blends, as presented in Figure 12 which would enable increased energy dissipation. At the 20% replacement level, the ternary blended fly ash and limestone mixtures also show

enhanced fracture behavior. This beneficial response is attributed primarily to the effects of limestone replacement as described above.

At the 35% replacement ratio (Figure 21(c)), a different trend is noted with respect to both peak load and post-peak behavior. The ternary blend of limestone and metakaolin shows similar peak load and post peak behavior as the OPC mix. The ternary blend of fly ash and limestone, on the other hand, shows a diminished peak load as well as post peak behavior. This is similar to the compressive strength response described in an earlier section. These observations can be attributed to the higher porosities and the fact that the pore structure is much less refined in this mixture at the testing age of 28 days. It would be expected that the ternary metakaolin blend at 35% OPC replacement should have higher toughness and residual load than the OPC control however this is not the case. The reason for the similar toughness but decrease in residual load is the fact that there is 15% more limestone present in this mixture which would have a strength decreasing effect on residual load but at the same time likely maintain the toughness due to the softer particle inclusion.

To better understand these effects, the results are plotted using toughness and residual load determined as outlined in Section 3.9.2. Figure 22 shows the values for the toughness and residual load of the different systems. The toughness of a material is the total work done or energy absorbed in the system, and residual load is a measure of the load present in the material post peak.

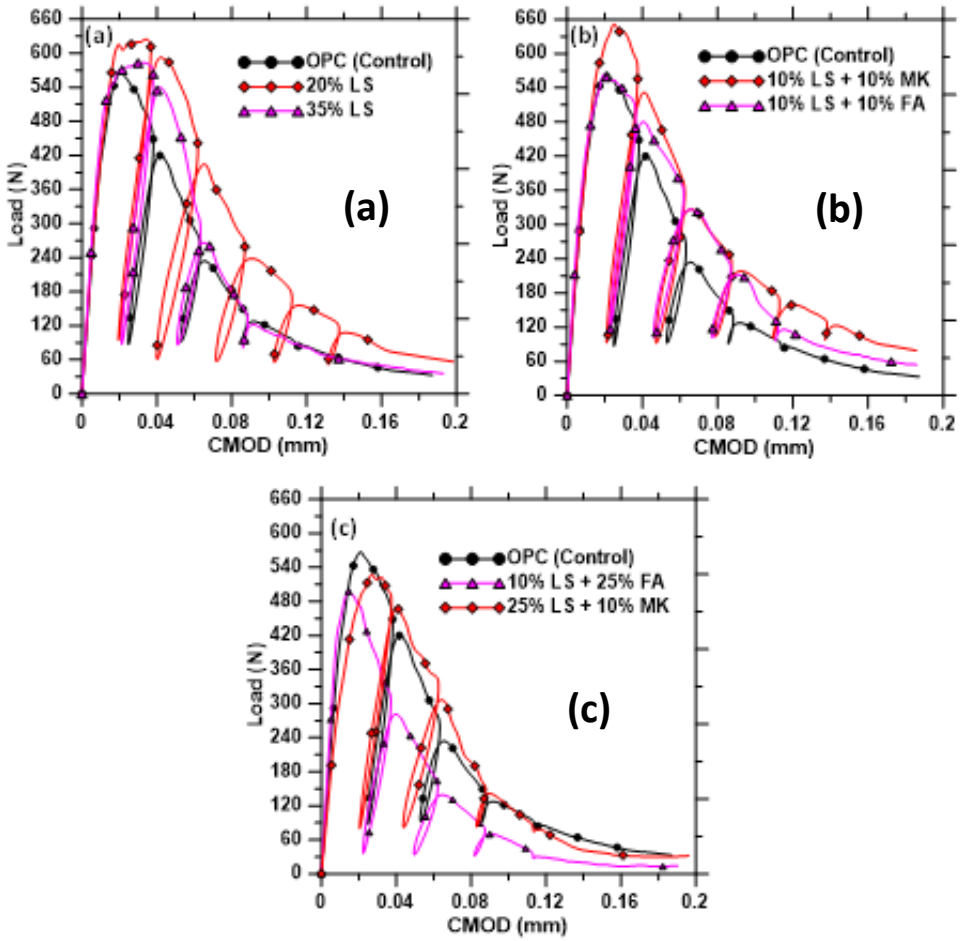

Figure 21: Load-CMOD responses for: (a) Binary LS, (b) 20% OPC replacement, (c) 35% OPC replacement

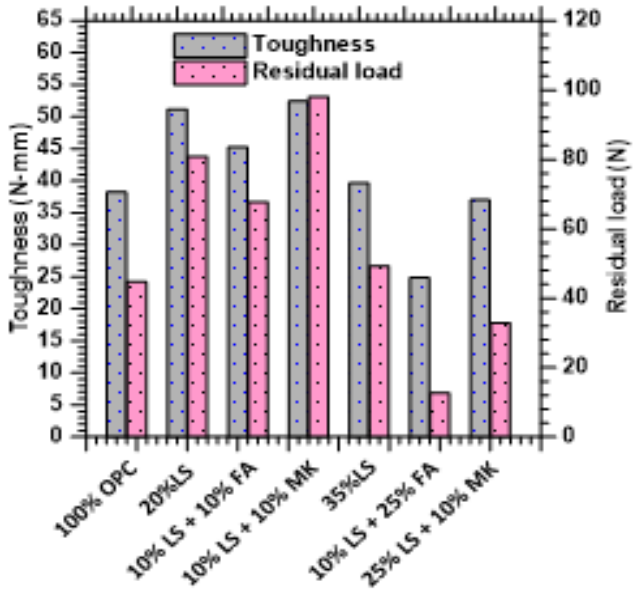

Figure 22: Toughness and residual load comparison

The fracture toughness and critical crack tip opening displacement were determined as presented in Section 3.9.2. Figure 23 shows the results of this analysis for the load-CMOD tests. Fracture toughness (K_{IC}) is a measure of the material's ability to resist fracture when an initial crack is present, and critical crack tip opening displacement ($CTOD_c$) is the limit after which unstable crack propagation will occur. For the 20% OPC replacement levels, the fracture toughness is higher than that of the OPC, which is a direct indication of the improved fracture performance because of the reasons described earlier. The pozzolanic reactions in the ternary blends at 20% OPC replacement levels with lower pore sizes demonstrates the depression of crack growth because of the synergistic effects causing densification of the microstructure. For the mixtures with a35% OPC replacement level, the fracture toughness values are comparable to those of the OPC control for the binary limestone and ternary fly ash blend.

The critical crack tip opening displacement is higher for the binary and ternary blends at both replacement levels compared to that of the OPC control. This is an indication of the increase in ductility when OPC is replaced by limestone or the other replacement materials used here. Increased ductility implies that softer limestone particle inclusions helps dissipate the energy required for a crack to propagate. A comparison of the fracture performance and the compressive strength results show that a higher ductility for binary and ternary blends is accompanied by a reduction in the compressive strength. The only exception is the 10% limestone 10% metakaolin blend which shows higher fracture and compressive properties than the control OPC.

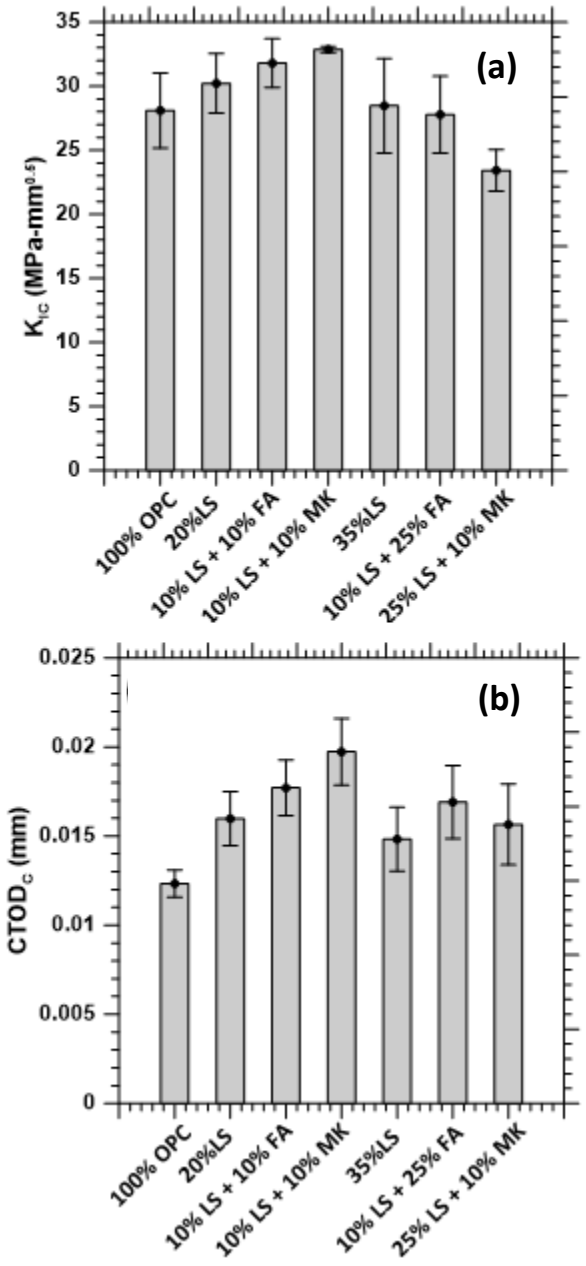

Figure 23: (a) Fracture toughness and (b) critical crack tip opening displacement of binary limestone and ternary blends at 20% and 35% OPC replacement

5. IONIC TRANSPORT IN TERNARY BLENDED CONCRETES

5.1. Electrical Impedance Spectra for the Chloride Transports Tests

The previous sections have outlined the type of reaction products formed and the resultant pore-structure and have attempted to relate these two factors to the mechanical and fracture behavior of the cementitious systems. Electrical impedance spectroscopy can provide an idea of the entire microstructure including the hydration products and pore network. Attempts on systems with replacement of OPC with an alumina species have been made to quantify the material microstructure through circuit models using the bulk arc in a Nyquist plot (J. Jain & Neithalath, 2011; Song, 2000). A Nyquist plot represents the frequency response from an AC-signal with the real part on the x-axis and the imaginary plot on the y-axis as described in section 3.7. An attempt is not made in this study to model the various components in the material microstructure, but only to observe the changes in the bulk resistance as a function of age and replacement type/level and to use the effective conductivities measured from the bulk resistances to determine a pore structure factor (a characteristic microstructural feature of the concretes). From the bulk resistance, the resistance of the percolating pores and the isolated pores can be determined. The measurement of uncertainty between duplicate measurements was less than 10% for the bulk resistance of specimens.

Figure 24 and 25 show the Nyquist plots (plots of real versus imaginary impedance) of the plain and modified concretes for 20% and 35% OPC replacement at 28 days and 56 days of curing before the NSSM test. During the hydration processes from 28 to 56 days the bulk resistance of the binary and ternary systems increases indicated in the shift to the right of the bulk arc (Dotelli & Mari, 2001). At 28 days the difference in bulk resistances

between the blended systems is an indication of the differences between their microstructures, which include the amount and type of hydration products and the pore structure. It is evident from the figures that both the ternary blends with limestone-metakaolin at both OPC replacement levels shows the highest bulk resistance at both ages. The greater amount of reaction products formed including the formation of carboaluminate phases in these mixtures is attributed to the densification of the microstructure indicated by the smaller pore sizes which have been previously described in sections 4.1 and 4.2, and are presented in Figure 12. At 28 days, 20% OPC replacement level for the binary limestone and fly ash, and the ternary fly ash blends show comparable bulk resistance values. It is not until 56 days that the binary fly ash, and ternary fly ash and metakaolin blends shift their bulk resistance to the right noticeably as more reaction products are expected to form at later ages. The slow pozzolanic reaction typical in fly ash is experienced here where there is a delay in the microstructure development from early ages to later ages. The significant microstructural improvement because of metakaolin addition, which was explained earlier can be noticed from the increased bulk resistances. However, it would also be prudent to note that incorporation of metakaolin into a concrete system reduces the pore solution conductivity, thereby increasing the bulk resistance. The resistance change denoted by the electrical impedance measurements are not solely due to the microstructural enhancements but contributed by the pore solution also.

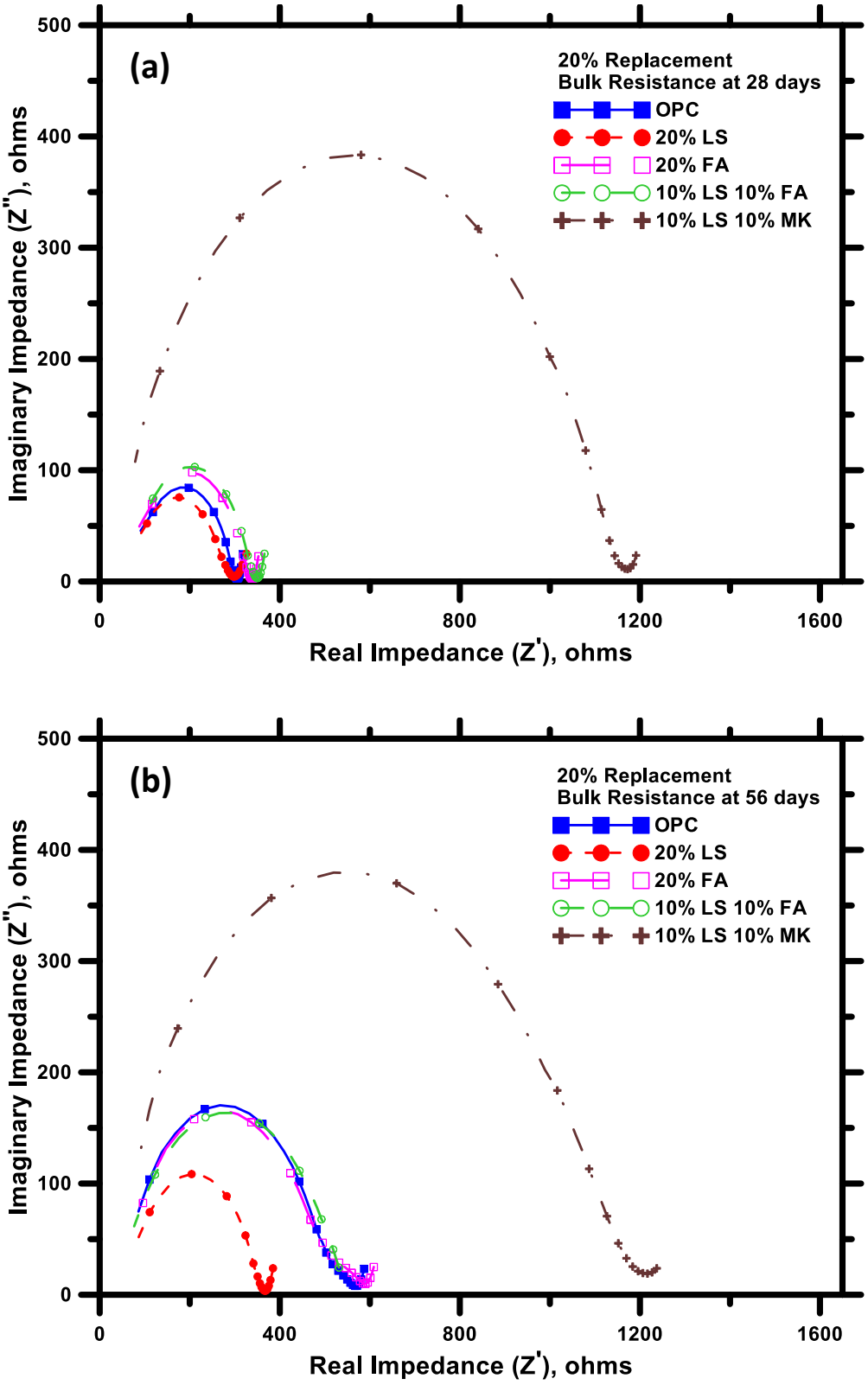

Figure 24: Electrical impedance spectra for 20% OPC replacement at: (a) 28 days and (b) 56 days

The microstructural development at later ages due to the increase in pozzolanic reactions is more evident in the 35% OPC replacement blends. The trends are similar for the bulk resistances at 28 days for both replacement levels except that the binary fly ash and ternary fly ash or metakaolin blends are clearly greater than those for the OPC control concrete. These same blends still show a larger bulk resistance than the OPC control concrete at 56 days with the ternary metakaolin blend showing the most pronounced increase. Focusing only on the fly ash binary and ternary blends at 20% OPC replacement is there a slight difference between their bulk resistances indicating that the microstructural changes taking place at 28 and 56 days are similar even with 10% limestone present in the ternary blend. The ternary blend containing 10% limestone and 25% fly ash shows a higher bulk resistance than the binary fly ash of 35% due to the synergistic effect between the larger volume fraction of fly ash combined with the lower volume fraction of limestone. Looking at the synergistic effect another way when there is a larger volume fraction of limestone (at 20%) and lower volume fraction of fly ash (at 15%) the bulk resistance is lower than the binary 35% fly ash. It has been shown that by choosing appropriate volume fractions between the limestone particles and an aluminate source the microstructure can be tailored to provide a synergistic benefit for a ternary blend containing limestone compared to a binary blend containing fly ash.

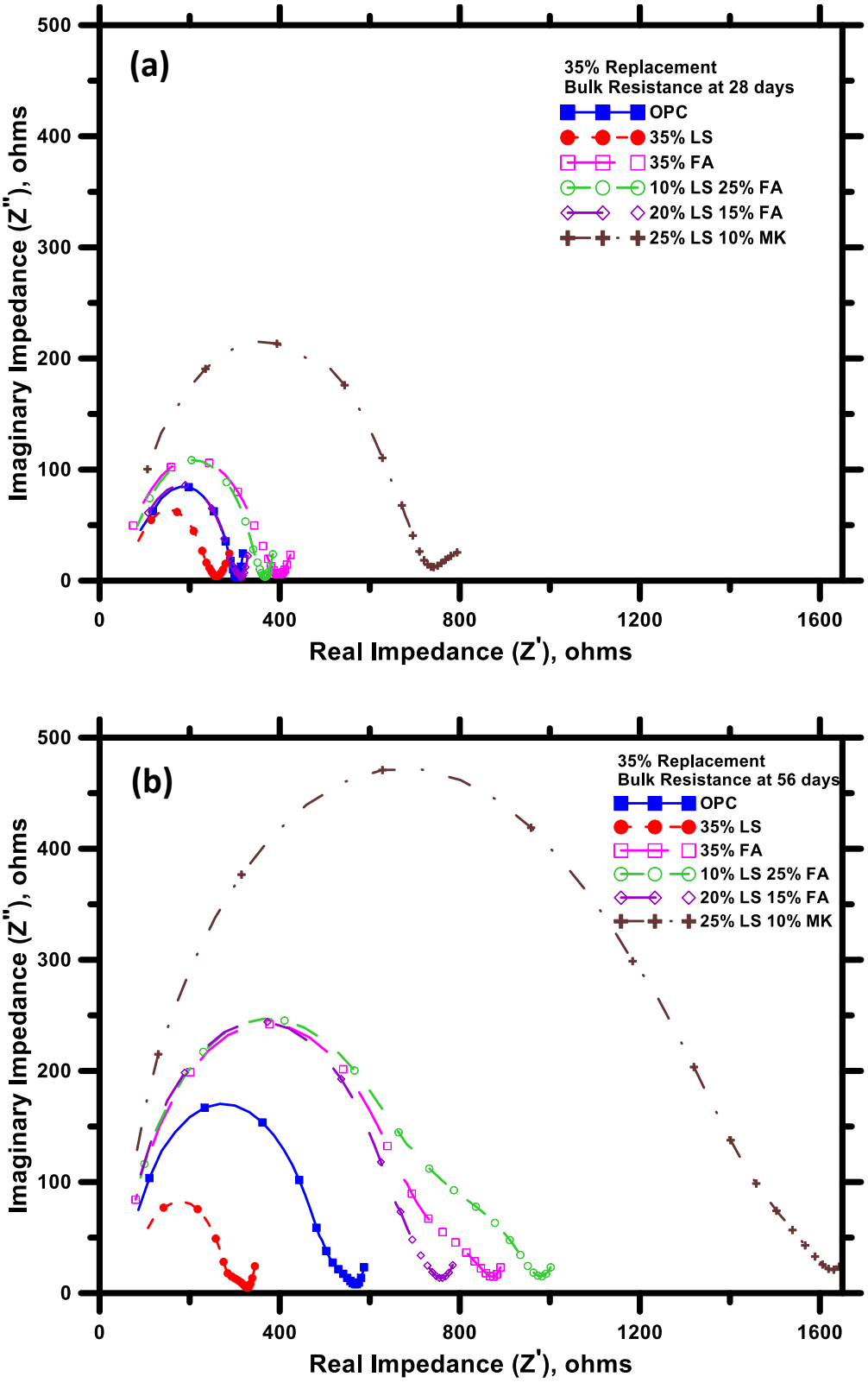

Figure 25: Electrical impedance spectra for 35% OPC replacement at: (a) 28 days and (b) 56 days

5.2. Rapid Chloride Permeability (RCP) Values

The RCP test is a conductivity (or resistivity) test to determine chloride transport through concrete. Since the test only measures the total charge passed through the sample, it lacks the ability to address certain microstructural changes that can occur due to the difference in pore network when different supplementary cementitious materials used, the pore solution in these systems, and the temperature increase that arise from the large electric potential (60V) applied to the specimen for just a short duration time of 6 hours (R. Feldman et al., 1999; C. Shi, 2004; Spiesz & Brouwers, 2012; Streicher & Alexander, 1995). Understanding the limitations of the test, this section describes a relative comparison between the RCP values of the different blends and the influence of OPC replacement levels. The RCP values of the binary and ternary blend concrete mixtures after 28 days of hydration were determined as described in section 3.8.2. Figure 26 shows the average RCP values, where the standard deviation ranged between 200 and 500 coulombs. The RCP values of the ternary blends are comparable to or lower than that of the control OPC concrete while the binary blends with limestone powder show values that are higher than that of the control OPC concrete. The synergy of limestone with fly ash or metakaolin, as explained in previous sections, is once again revealed here. One of the most significant aspects is the dramatic reduction in the RCP values of the ternary blends containing metakaolin. In line with the discussions in the previous sections, the likely cause of lower RCP values is mostly due to: (a) pozzolanic reactions and (b) the formation of carboaluminate phases which was explained in section 4.1. However, these mixtures also have a lower pore solution conductivity due to the lower amounts of alkalis in metakaolin as compared to fly ash as noted in Table 1.

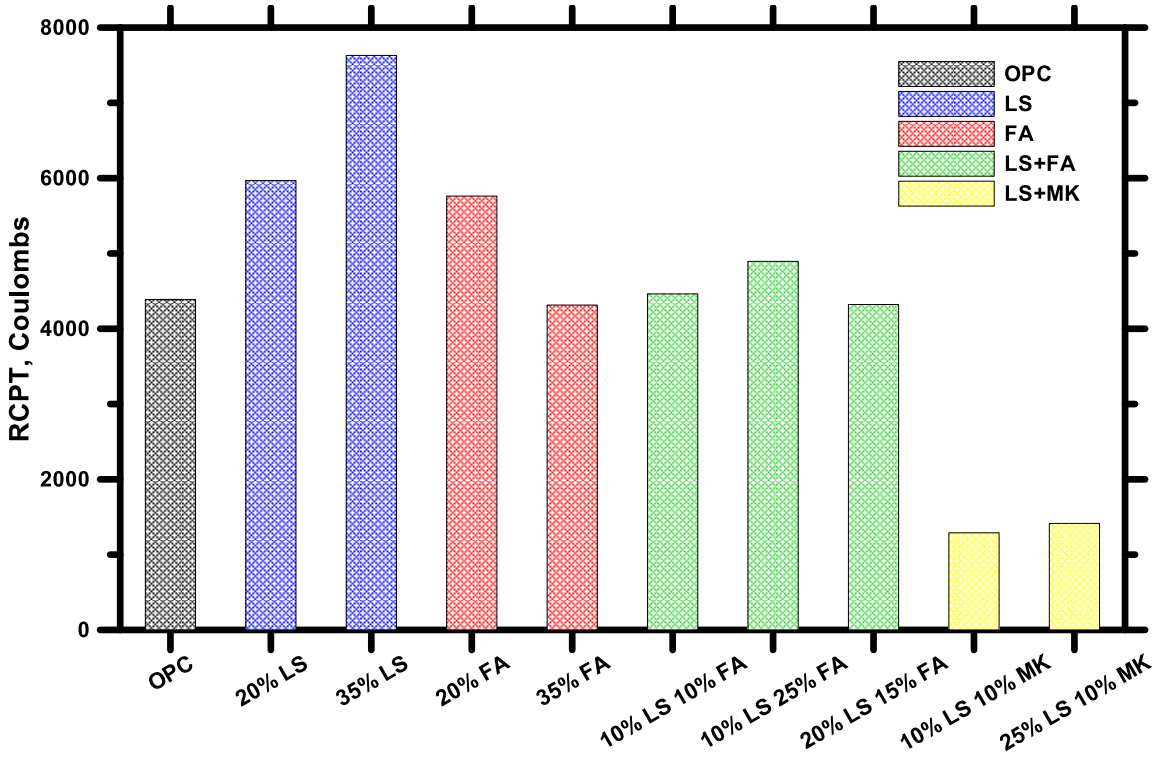

Figure 26: RCP values at 28 days for 20% and 35% OPC replacement levels

Figure 27 shows the linear relationship between the charge passed in the RCP test on binary and ternary blends normalized by the charge passed through the control OPC concrete, and the bulk electrical conductivity of these concretes measured before the start of the RCP test, for concretes containing 20% and 35% of OPC replacement materials. It should again be stated that the RCP test is basically an electrical conductivity (or resistivity) test and that it does adequately represent the microstructural characteristics of concrete (R. Feldman et al., 1999; J. A. Jain & Neithalath, 2010; Julio-Betancourt & Hooton, 2004). The fact that the RCP test is a conductivity test is evident from the relationship shown in Figure 27.

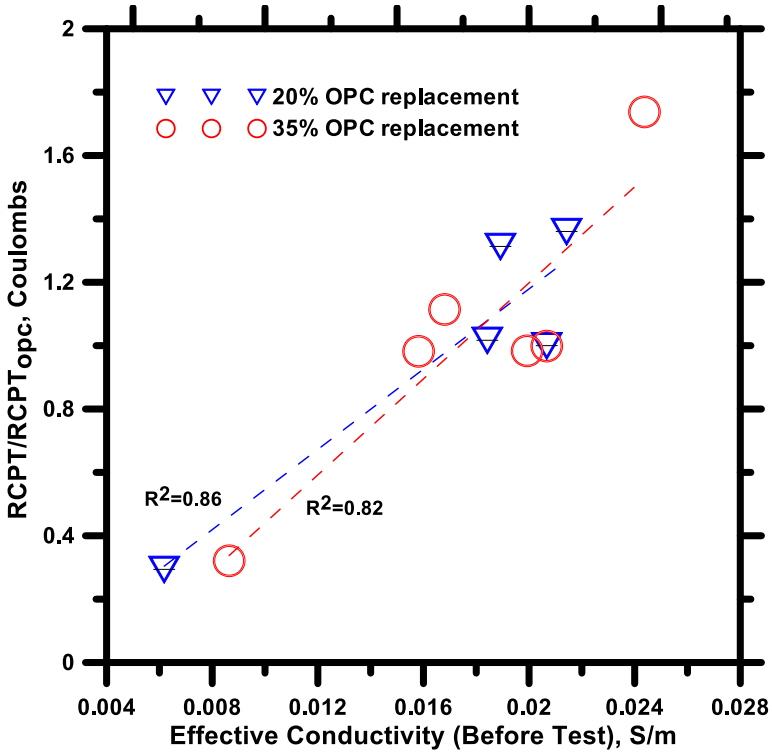

Figure 27: Relationship between effective conductivity and normalized RCP values

5.3. Non-Steady-State Migration (NSSM) for Chloride Transport Representation

The NSSM test provides a better indication of the chloride transport parameters in an accelerated migration test. The NSSM test is an indirect means to determine the chloride transport resistance of concretes but is more indicative of the nature of the pore structure due to the lower applied voltage (and Joule heating) and longer test duration (J. Jain & Neithalath, 2011; Julio-Betancourt & Hooton, 2004). Figure 28 shows the average NSSM coefficients for the systems with 20% and 35% replacement of OPC respectively, at hydration times of 28 and 56 days. Note that the standard deviation range at 28 days is 0.1-0.6 ($x10^{-12}$, m^2/s) and at 56 days is 0.1-0.8 ($x10^{-12}$, m^2/s). The NSSM coefficients are comparable to/lower than that of the OPC concrete for systems with a replacement level of 20%. In line with the strength and RCP results, the ternary blend concrete where 20% of

OPC is replaced by limestone and metakaolin has the lowest NSSM coefficient, which is about 60% lower than that of the control concrete. Even at the 35% replacement level, the limestone-metakaolin blend shows a lower NSSM coefficient at 28 days and an even lower NSSM coefficient at 56 days which is about 40% lower than that of the control concrete. At both replacement levels the ternary blend containing limestone and fly ash has a higher NSSM coefficient than the binary fly ash blend concrete, but a value lower than the binary limestone blend concrete.

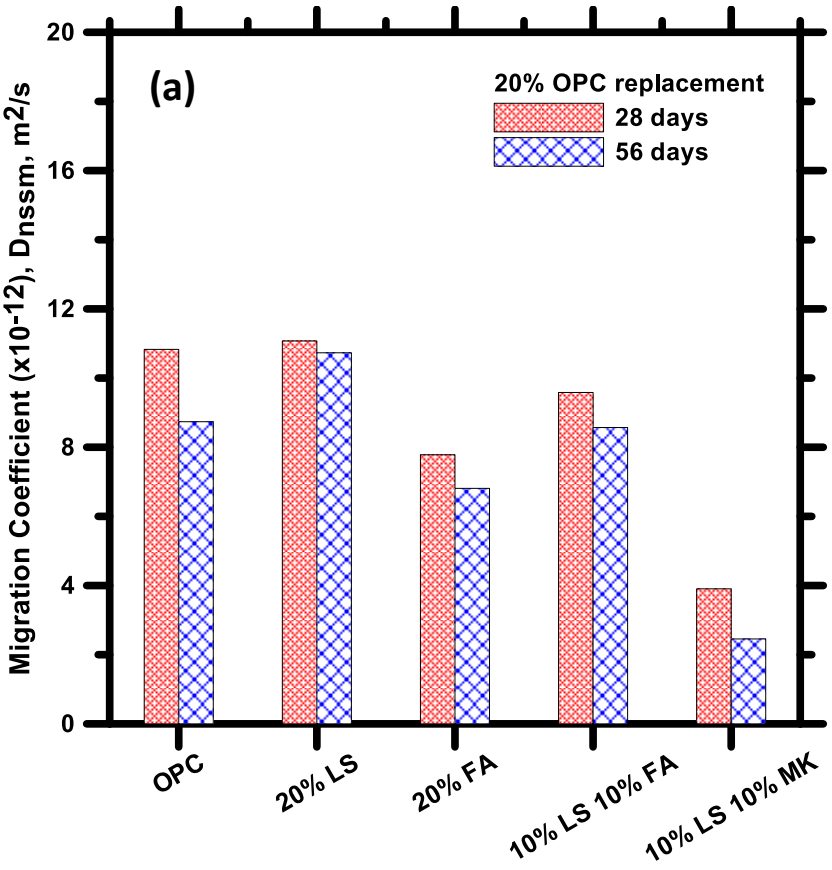

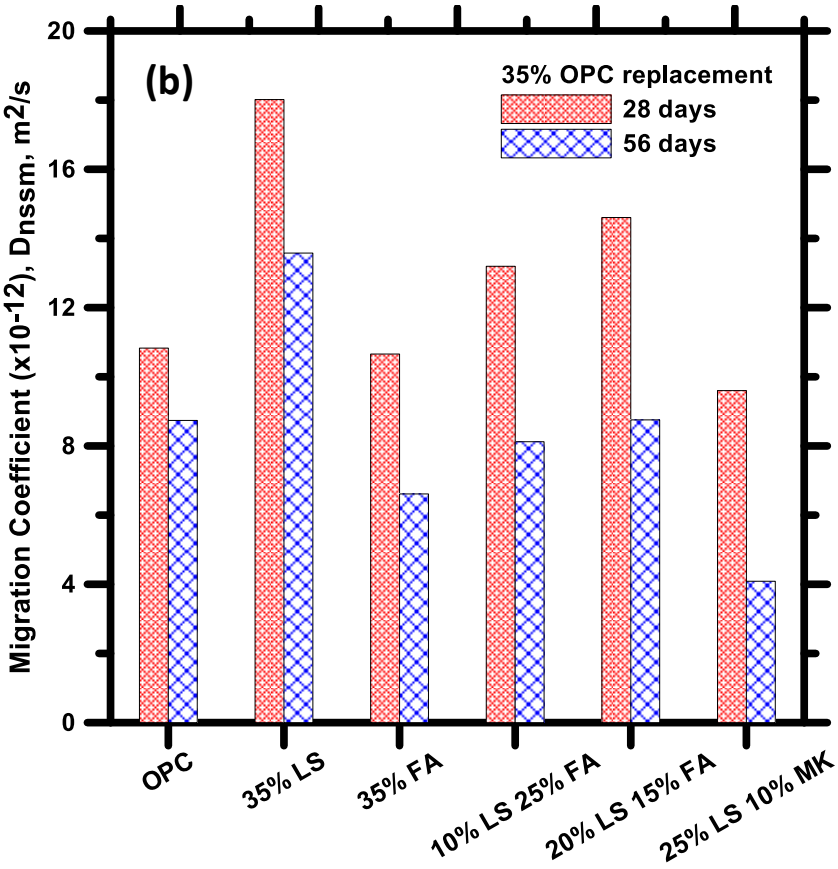

Figure 28: Non-steady-state migration coefficient values for: (a) 20% OPC replacement and (b) 35% OPC replacement

At an OPC replacement level of 35%, the NSSM migration coefficients at 28 days are generally higher than that of the control concrete, while at 56 days, they are comparable to/lower than the OPC concrete except for the binary limestone blend. The later age pozzolanic reactions attribute to the lower NSSM coefficients at later ages due to pore structure refinement. The NSSM coefficients reported here show that it is possible to proportion concretes containing limestone with high levels of OPC replacement, which are capable of providing durability performance equivalent to or better than pure OPC concretes. It should be noted that limestone powders of two different sizes (d_{50} = 3 µm and

10 μm) were blended in this study to provide the OPC-limestone blend with a particle size distribution that is similar to that of the OPC. If a finer limestone powder (for example, one with a d_{50} = 0.7 μm) is used as part of the total limestone content in concrete, the performance from the durability aspect may be further enhanced due to an increase in the maximum packing density. The synergistic improvements in the hydration and reaction product formation of these blended systems as outlined in section 4.1 can be expected to result in improved durability performance of these concretes.

The relationship between the conductivity of the concretes before the NSSM test and the normalized NSSM coefficients (NSSM coefficients of the binary or ternary blends divided by that of the OPC concrete) after 28 and 56 days of hydration is shown in Figure 29. Two separate trends corresponding to the two distinct OPC replacement levels are observed. Although there is correlation between the normalized NSSM coefficients and the specimen conductivity, it is weaker than those for the RCP test results noted in Figure 27. The reason behind this weakness is the NSSM test does not just measure the charge passed, but rather describes the migration of Cl^- ions under an applied electrical potential.

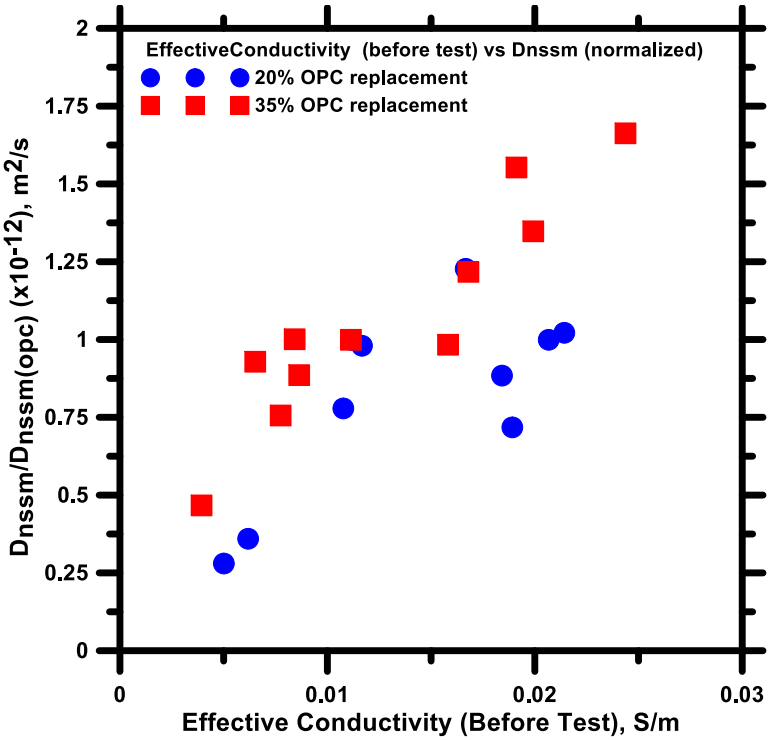

Figure 29: Relationship between effective conductivity and the non-steady-state migration coefficient

5.4. Relationship between pore structure features and chloride migration parameters

A relationship exists between the pore solution conductivity (σ_0) and a pore structure factor to the bulk specimen conductivity. The pore structure factor is defined as the product of porosity (Φ) and a pore connectivity (β) (Christensen et al., 1994; Garboczi, 1990; Neithalath, Weiss, & Olek, 2006; Sanish, Neithalath, & Santhanam, 2013) as:

$$\sigma_{eff} = \sigma_0 \Phi \beta \qquad (5.4\text{-}1)$$

The conductivity of the pore solution was predicted using the concentrations of Na^+, K^+, and OH^- in the solution. The concentrations of alkali ions in the solution were obtained using the model developed by Taylor (Taylor, 1987):

$$C_i = \frac{n_i^r}{V_w + b_{a_i} \cdot F} \quad (5.4\text{-}2)$$

Where n_i^r is the total amount of alkali ions in the bound products and moles in the solution, V_w is the volume of the pore solution, b_{a_i} is a binding factor of the alkali ion, and F is the fraction between the quantity of hydration products able to consume alkali cations in the paste.

The pore solution conductivity was determined using the concentrations of the alkali ions from (5.4-2) as a weighted sum of equivalent conductivities of each alkaline ionic species (Snyder, Feng, Keen, & Mason, 2003):

$$\sigma_0 = \sum_i z_i c_i \Lambda_i \quad (5.4\text{-}3)$$

Where Λ_i the equivalent ionic conductivities of these species at infinite dilution, z is the species valence and c is the molar of alkali concentrations also described in (Snyder et al., 2003; Taylor, 1987). Table 4 shows that initial concentration of alkali ions present in the blended systems at both replacement levels along with the calculated pore solution conductivity.

Table 4: Alkali ionic species and pore solution conductivity present at 28 days of hydration

Mixture	Pore solution composition (mmol/L)			Pore solution conductivity (σ_0), S/m
	K^+	Na^+	OH^-	
Plain	210	150	360	7.57
LS 20	160	110	270	5.93
FA 20	250	300	550	11.00
LS 10 FA 10	210	210	420	8.58
LS 10 MK 10	150	100	250	5.34
LS 35	120	80	210	4.57
FA 35	270	390	660	12.77
LS 10 FA 25	230	310	540	10.62
LS 20 FA 15	190	220	410	8.33
LS 25 MK 10	110	80	190	4.24

The average pore structure factor ($\phi\beta$) determined for the binary and ternary blends is shown in Figure 30(a). A higher pore structure factor indicates a lower resistance to ionic transport. Expectedly, the two mixtures that display the highest pore structure factors than the control OPC concrete are the binary limestone blends having 20% and 35% OPC replacement. This effect is attributed to: (a) the depressed pore solution conductivity of

these mixtures, and (b) the effects of dilution being dominant over the filler effect: in agreement with the strength and Cl^- results reported previously. Section 4.2, Figure 12(a) showed the large volume of mercury intruded with the 35% having the largest amount of all mixes which is also shown by the pore structure factor in Figure 30(a). The binary OPC-fly ash blend demonstrates a much lower pore structure factor at 56 days of hydration, demonstrating the effects of pozzolanic reactivity. The ternary blend with a 20% OPC replacement containing limestone and metakaolin has the lowest pore structure factor, while ternary blends containing limestone and fly ash also have values significantly lower than that of the OPC concretes, showing the synergistic influence of these replacement materials.

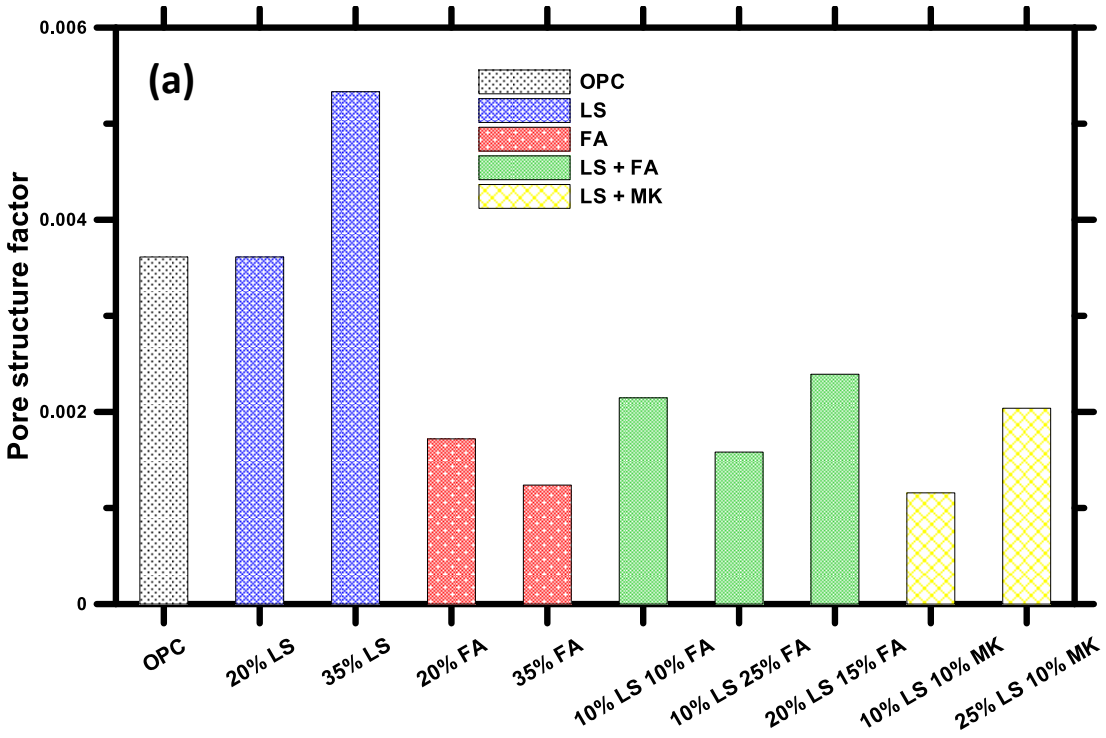

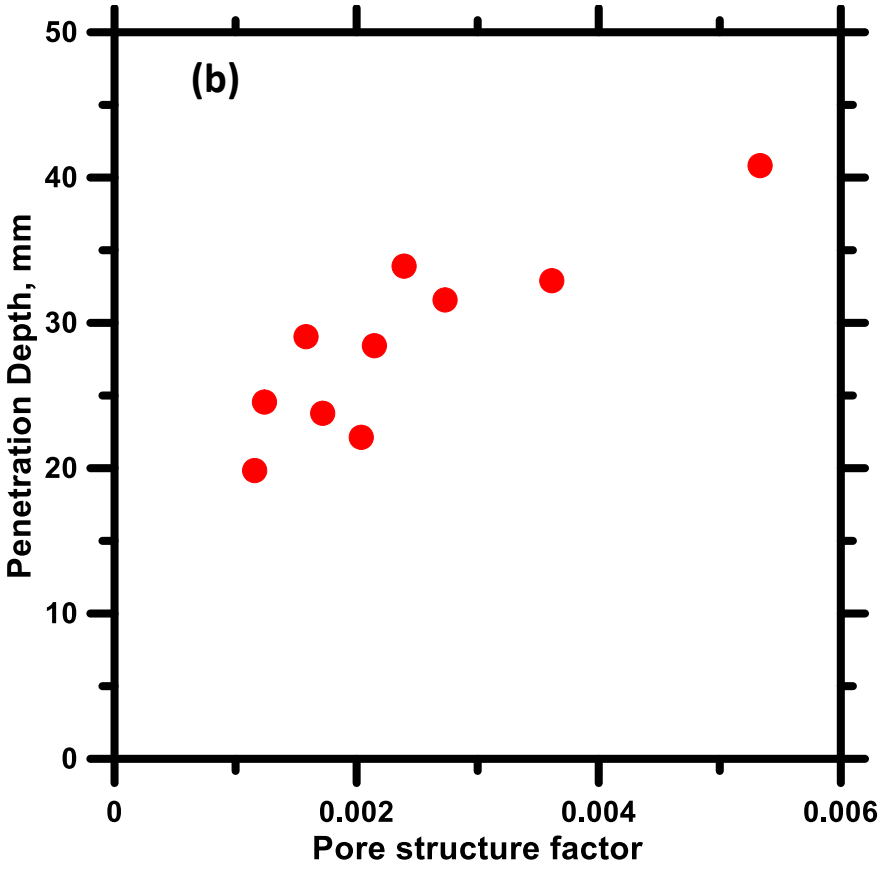

Figure 30: (a) Pore structure factors of all concrete mixtures before the NSSM test, and (b) the relationship between the pore structure factor and Cl^- penetration depths after the NSSM test

The pore structure factor described above is influential in dictating the movement of moisture and ionic species through concrete. Figure 30(b) shows the relationship between the pore structure factor and the Cl^- penetration depth determined using the colorimetric technique after 24 hours of NSSM test. A good relationship is observed, indicating that the pore structure factor obtained from EIS measurements before the NSSM test is a reliable indicator of the extent of penetration of chloride ions. Since the NSSM coefficient is highly dependent on the measured penetration depths, determinations of pore structure factor before the test facilitates reasonable comparisons of the transport behaviors of concretes.

In Figure 31, there is an obvious relationship between the pore structure factor before the start of the NSSM test and the NSSM migration coefficient. The relationship is much stronger for the NSSM migration coefficient than the chloride penetration depth due to the migration coefficient being a function not only of the penetration depth but also the voltage applied, temperature, and testing duration outlined in section 3.8.3. The three points that deviate from the linear trend are the 35% OPC replacement fly ash binary and ternary samples. At 28 days the pore structure of these samples are less refined compared to the other blends because of the slower pozzolanic reaction discussed in section 4.1 and the higher pore solution conductivities for reasons explained earlier in this section.

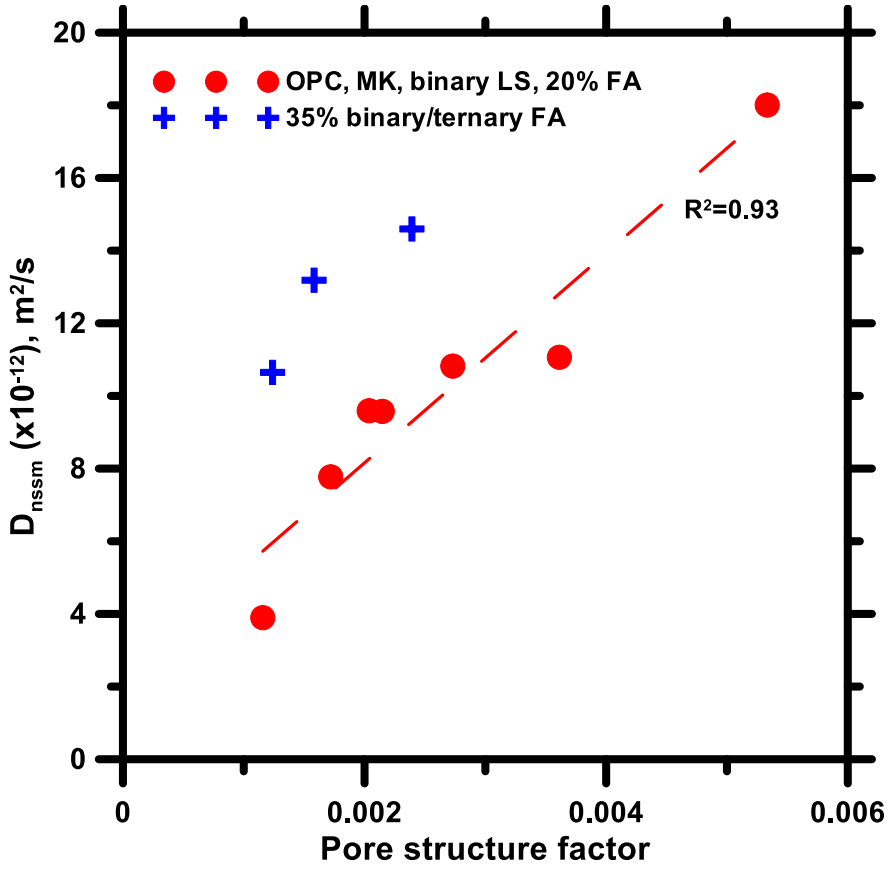

Figure 31: Relationship between the pore structure factor before the NSSM test and D_{nssm}

Figure 32 shows the relationship between the conductivities of the concretes before and after the NSSM test. The conductivities are generally lower after the NSSM test (J. A. Jain & Neithalath, 2010; J. Jain & Neithalath, 2011). The reduction in the conductivity is attributed to a reduction in the conductivity of the pore solution because the ingress of Cl^- ions replaces some of the (higher mobility) OH^- ions in solution. It is also conceivable that the pore structure factor would be reduced after the migration test if Cl^- ions are bound in the hydration products, which upon formation precipitate in the pore space, complicating the pore topology. As such, assuming that the overall pore volume does not significantly change during the migration test (Sánchez, Nóvoa, de Vera, & Climent, 2008), it is the connectivity of pore channels that is reduced when the chloroaluminate hydrates are deposited on the pore walls (Balonis et al., 2010; J. Jain & Neithalath, 2011; Sánchez et al., 2008). Equivalent circuit models for electrical impedance spectra have established such behaviors where the capacitance of the solid-pore interface was observed to increase after the migration test (J. Jain & Neithalath, 2011; Sánchez et al., 2008). It should be noted that while previous studies (Castellote, Andrade, & Alonso, 1999; Spiesz, Ballari, & Brouwers, 2012) have reported that Cl^- ions are indeed bound into the reaction products during a non-steady state migration test, there is some debate about the relative rates of the chemical reaction and ionic transport and how these may influence binding (Samson, Marchand, & Snyder, 2003).

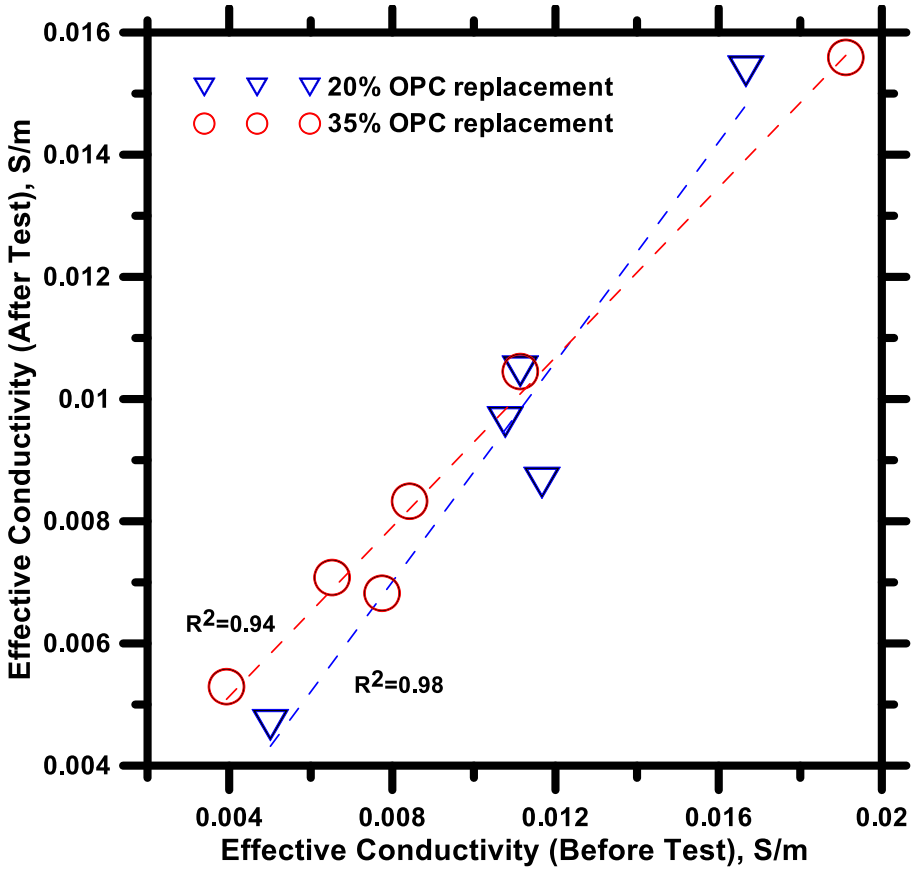

Figure 32: Effective conductivities before and after the NSSM test at 56 days

6. CONCLUSIONS

6.1. Mechanical Performance

The effects of limestone incorporation and synergistic effect of limestone and fly ash or metakaolin on fracture behavior of cement mortars are investigated in this study. Based on the results of this investigation, the following conclusions can be drawn:

(i) Incorporation of limestone powder (replacing 20% by volume of OPC) gives slightly lower compressive strength than the OPC mortar but improves the fracture behavior of the system. 20% replacement by limestone powder yields a 7.5% increase in fracture toughness (K_{IC}), and a 29.5% increase in $CTOD_c$ at 28 days.

(ii) Synergy between limestone and metakaolin or limestone, proved previously to be beneficial in terms of strength, provides improved fracture characteristics. For 20% replacement levels, ternary blends containing metakaolin or fly ash as third phase performs significantly better as compared to the OPC-limestone binary blend due to the additional pozzolanic reactivity. For the blend containing 80% OPC, 10% limestone and 10% metakaolin an increase of 17% in K_{IC} and 60% in $CTOD_c$ is observed over 100% OPC mortar.

(iii) For higher replacement levels (35% by volume) , the compressive strengths were found to be significantly lower as compared to OPC mortar although it gives improved performance in terms of unstable crack-propagation threshold limit ($CTOD_c$). The fracture toughness in the systems with 35% OPC replacement were found to be equal or slightly lower as compared to 100% OPC control sample. Incorporation of 10% limestone and 25% fly ash by volume in

a ternary blend results in about 20% reduction in compressive strength (even though the compressive strengths (40-45 MPa) are suitable for most of the construction applications) whereas the $CTOD_c$ increases by 37% while keeping the reduction in K_{IC} below 1%. In light of this result, it is stated that the fracture properties of cement-based systems are not functions of its mechanical properties only and the constitution of cementitious materials should be reconsidered.

6.2. Ionic Transport

Detailed understanding of Cl^- ion transport in binary and ternary blend concretes using accelerated ionic migration tests have been reported here. Limestone powder along with fly ash or metakaolin were used as OPC replacement materials, with a total of 20% or 35% of OPC by volume being replaced. Binary blends containing limestone showed higher RCP and NSSM values than the OPC (control) system, while the ternary blends containing limestone and fly ash or metakaolin showed comparable or lower RCP (and NSSM) values. When the OPC replacement was 20%, the binary and ternary blends showed comparable or lower migration coefficients than the OPC concrete, while at 35% replacement level, the ternary blend with metakaolin showed lower values than the control concrete. The beneficial synergy of limestone and metakaolin, which were observed in the mechanical property development of concretes, is also evident from migration results. Electrical conductivity measurements carried out before the NSSM test, are integrated with solution conductivity details to determine a pore structure factor, which demonstrated a strong correlation with the penetration depth of Cl^- ions and the NSSM migration coefficient. Thus

the pore structure factor can be used to compare the transport performance of different concretes.

WORK CITED

Abell, A. B., Willis, K. L., & Lange, D. A. (1999). Mercury Intrusion Porosimetry and Image Analysis of Cement-Based Materials. *Journal of Colloid and Interface Science*, *211*(1), 39–44. doi:10.1006/jcis.1998.5986

Ali, M. B., Saidur, R., & Hossain, M. S. (2011). A review on emission analysis in cement industries. *Renewable and Sustainable Energy Reviews*, *15*(5), 2252–2261. doi:10.1016/j.rser.2011.02.014

Almusallam, A. A. (2001). Effect of degree of corrosion on the properties of reinforcing steel bars. *Construction and Building Materials*, *15*(8), 361–368. doi:10.1016/S0950-0618(01)00009-5

Antoni, M., Rossen, J., Martirena, F., & Scrivener, K. (2012). Cement substitution by a combination of metakaolin and limestone. *Cement and Concrete Research*, *42*(12), 1579–1589. doi:10.1016/j.cemconres.2012.09.006

Aranda Usón, A., López-Sabirón, A. M., Ferreira, G., & Llera Sastresa, E. (2013). Uses of alternative fuels and raw materials in the cement industry as sustainable waste management options. *Renewable and Sustainable Energy Reviews*, *23*, 242–260. doi:10.1016/j.rser.2013.02.024

ASTM C109 / C109M - 13. Standard Test Method for Compressive Strength of Hydraulic Cement Mortars (Using 2-in. or 50-mm Cube Specimens). (2013). *ASTM International, West Conshohocken, PA (2013)*.

ASTM C1202 - 12. Standard Test Method for Electrical Indication of Concrete's Ability to Resist Chloride Ion Penetration. (2012). *ASTM International, West Conshohocken, PA (2012)*.

ASTM C150 / C150M - 12. Standard Specification for Portland Cement. (2012). *ASTM International, West Conshohocken, PA (2012)*.

ASTM C1609 / C1609 - 12. Standard Test Method for Flexural Performance of Fiber-Reinforced Concrete (Using Beam With Third-Point Loading). (2012). *ASTM International, West Conshohocken, PA (2012)*.

ASTM C1714 / C1714M - 13a. Standard Specification for Preblended Dry Mortar Mix for Unit Masonry. (2013). *ASTM International, West Conshohocken, PA (2013)*.

ASTM C192 / C192M - 13a. Standard Practice for Making and Curing Concrete Test Specimens in the Laboratory. (2013). *ASTM International, West Conshohocken, PA (2013)*.

ASTM C305 - 13. Standard Practice for Mechanical Mixing of Hydraulic Cement Pastes and Mortars of Plastic Consistency. (2013). *ASTM International, West Conshohocken, PA (2013)*.

ASTM C39 / 39M -14. Standard Test Method for Compresive Strength of Cylindrical Concrete Specimens. (2014). *ASTM International, West Conshohocken, PA (2014)*.

ASTM C494 / C494M - 13. Standard Specification for Chemical Admixtures for Concrete. (2013). *ASTM International, West Conshohocken, PA (2013)*.

ASTM C568 / C568 - 10. Standard Specification for Limestone Dimension Stone. (2010), *ASTM International, West Conshohocken, PA (2010)*.

ASTM C618-12a. Standard Specification for Coal Fly Ash and Raw or Calcined Natural Pozzolan for Use in Concrete. (2012). *ASTM International, West Conshohocken, PA (2012)*.

ASTM C78 / C78M - 10e1. Standard Test Method for Flexural Strength of Concrete (Using Simple Beam With Third-Point Loading). (2010). *ASTM International, West Conshohocken, PA (2010)*.

Atahan, H. N., Oktar, O. N., & Taşdemir, M. A. (2009). Effects of water–cement ratio and curing time on the critical pore width of hardened cement paste. *Construction and Building Materials*, *23*(3), 1196–1200. doi:10.1016/j.conbuildmat.2008.08.011

Balonis, M., Lothenbach, B., Le Saout, G., & Glasser, F. P. (2010). Impact of chloride on the mineralogy of hydrated Portland cement systems. *Cement and Concrete Research*, *40*(7), 1009–1022. doi:10.1016/j.cemconres.2010.03.002

Bažant, Z. P. (2002). Concrete fracture models: testing and practice. *Engineering Fracture Mechanics*, *69*(2), 165–205. doi:10.1016/S0013-7944(01)00084-4

Bažant, Z. P., & Gettu, R. (1992). Rate Effects and Load Relaxation in Static Fracture of Concrete. *Materials Journal*, *89*(5), 456–468.

Bentz, D. P., Hansen, A. S., & Guynn, J. M. (2011). Optimization of cement and fly ash particle sizes to produce sustainable concretes. *Cement and Concrete Composites*, *33*(8), 824–831. doi:10.1016/j.cemconcomp.2011.04.008

Bentz, D. P., Sato, T., de la Varga, I., & Weiss, W. J. (2012). Fine limestone additions to regulate setting in high volume fly ash mixtures. *Cement and Concrete Composites*, *34*(1), 11–17. doi:10.1016/j.cemconcomp.2011.09.004

Berry, E. E., Hemmings, R. T., & Cornelius, B. J. (1990). Mechanisms of hydration reactions in high volume fly ash pastes and mortars. *Cement and Concrete Composites*, *12*(4), 253–261. doi:10.1016/0958-9465(90)90004-H

Bonavetti, V., Donza, H., Menéndez, G., Cabrera, O., & Irassar, E. F. (2003). Limestone filler cement in low w/c concrete: A rational use of energy. *Cement and Concrete Research*, *33*(6), 865–871. doi:10.1016/S0008-8846(02)01087-6

Bonavetti, V. L., Rahhal, V. F., & Irassar, E. F. (2001). Studies on the carboaluminate formation in limestone filler-blended cements. *Cement and Concrete Research*, *31*(6), 853–859. doi:10.1016/S0008-8846(01)00491-4

Cam, H. T., & Neithalath, N. (2010). Moisture and ionic transport in concretes containing coarse limestone powder. *Cement and Concrete Composites*, *32*(7), 486–496. doi:10.1016/j.cemconcomp.2010.04.002

Capozucca, R. (1995). Damage to reinforced concrete due to reinforcement corrosion. *Construction and Building Materials*, *9*(5), 295–303. doi:10.1016/0950-0618(95)00033-C

Cassagnabère, F., Diederich, P., Mouret, M., Escadeillas, G., & Lachemi, M. (2013). Impact of metakaolin characteristics on the rheological properties of mortar in the fresh state. *Cement and Concrete Composites*, *37*, 95–107. doi:10.1016/j.cemconcomp.2012.12.001

Castellote, M., Andrade, C., & Alonso, C. (1999). Chloride-binding isotherms in concrete submitted to non-steady-state migration experiments. *Cement and Concrete Research*, *29*(11), 1799–1806. doi:10.1016/S0008-8846(99)00173-8

Celik, K., Jackson, M. D., Mancio, M., Meral, C., Emwas, A.-H., Mehta, P. K., & Monteiro, P. J. M. (2014). High-volume natural volcanic pozzolan and limestone powder as partial replacements for portland cement in self-compacting and sustainable concrete. *Cement and Concrete Composites*, *45*, 136–147. doi:10.1016/j.cemconcomp.2013.09.003

Celik, K., Meral, C., Mancio, M., Mehta, P. K., & Monteiro, P. J. M. (n.d.). A comparative study of self-consolidating concretes incorporating high-volume natural pozzolan or high-volume fly ash. *Construction and Building Materials*. doi:10.1016/j.conbuildmat.2013.11.065

Chen, J. J., Kwan, A. K. H., & Jiang, Y. (2014). Adding limestone fines as cement paste replacement to reduce water permeability and sorptivity of concrete. *Construction and Building Materials*, *56*, 87–93. doi:10.1016/j.conbuildmat.2014.01.066

Christensen, B. J., Coverdale, R. T., Olson, R. A., Ford, S. J., Garboczi, E. J., Jennings, H. M., & Mason, T. O. (1994). Impedance spectroscopy of hydrating cement based materials: measurement, interpretation and application. *Journal of the American Ceramic Society*, *77*, 2789–2804.

Cook, R. A., & Hover, K. C. (1999). Mercury porosimetry of hardened cement pastes. *Cement and Concrete Research*, *29*(6), 933–943. doi:10.1016/S0008-8846(99)00083-6

Courard, L., & Michel, F. (2014). Limestone fillers cement based composites: Effects of blast furnace slags on fresh and hardened properties. *Construction and Building Materials*, *51*, 439–445. doi:10.1016/j.conbuildmat.2013.10.076

D P Bentz, E. F. I. (2009). Limestone Fillers Conserve Cement Part 2: Durability Issues and the Effects of Limestone Fineness on Mixtures. *Concrete International*, *31*(12), 35–39.

Darweesh, H. H. M. (2004). Limestone as an accelerator and filler in limestone-substituted alumina cement. *Ceramics International*, *30*(2), 145–150. doi:10.1016/S0272-8842(03)00073-7

De Weerdt, K., Haha, M. B., Le Saout, G., Kjellsen, K. O., Justnes, H., & Lothenbach, B. (2011). Hydration mechanisms of ternary Portland cements containing limestone powder and

fly ash. *Cement and Concrete Research*, *41*(3), 279–291. doi:10.1016/j.cemconres.2010.11.014

De Weerdt, K., Kjellsen, K. O., Sellevold, E., & Justnes, H. (2011). Synergy between fly ash and limestone powder in ternary cements. *Cement and Concrete Composites*, *33*(1), 30–38. doi:10.1016/j.cemconcomp.2010.09.006

Deschner, F., Winnefeld, F., Lothenbach, B., Seufert, S., Schwesig, P., Dittrich, S., … Neubauer, J. (2012). Hydration of Portland cement with high replacement by siliceous fly ash. *Cement and Concrete Research*, *42*(10), 1389–1400. doi:10.1016/j.cemconres.2012.06.009

Díaz, B., Nóvoa, X. R., & Pérez, M. C. (2006). Study of the chloride diffusion in mortar: A new method of determining diffusion coefficients based on impedance measurements. *Cement and Concrete Composites*, *28*(3), 237–245. doi:10.1016/j.cemconcomp.2006.01.009

Domone, P. L. (2007). A review of the hardened mechanical properties of self-compacting concrete. *Cement and Concrete Composites*, *29*(1), 1–12. doi:10.1016/j.cemconcomp.2006.07.010

Dotelli, G., & Mari, C. M. (2001). The evolution of cement paste hydration process by impedance spectroscopy. *Materials Science and Engineering: A*, *303*(1–2), 54–59. doi:10.1016/S0921-5093(00)01886-4

Dweck, J., Buchler, P. M., Coelho, A. C. V., & Cartledge, F. K. (2000). Hydration of a Portland cement blended with calcium carbonate. *Thermochimica Acta*, *346*(1–2), 105–113. doi:10.1016/S0040-6031(99)00369-X

Fang, C., Lundgren, K., Chen, L., & Zhu, C. (2004). Corrosion influence on bond in reinforced concrete. *Cement and Concrete Research*, *34*(11), 2159–2167. doi:10.1016/j.cemconres.2004.04.006

Feldman, R. F., Carette, G. G., & Malhotra, V. M. (1990). Studies on mechanics of development of physical and mechanical properties of high-volume fly ash-cement pastes. *Cement and Concrete Composites*, *12*(4), 245–251. doi:10.1016/0958-9465(90)90003-G

Feldman, R., Prudencio Jr., L. R., & Chan, G. (1999). Rapid chloride permeability test on blended cement and other concretes: correlations between charge, initial current and conductivity. *Construction and Building Materials*, *13*(3), 149–154. doi:10.1016/S0950-0618(98)00033-6

FHWA. (2002). *Corrosion Costs and Preventive Strategies in the United States* (No. FHWA-RD-01-156). Federal Highway Administration.

Fraay, A. L. A., Bijen, J. M., & de Haan, Y. M. (1989). The reaction of fly ash in concrete a critical examination. *Cement and Concrete Research*, *19*(2), 235–246. doi:10.1016/0008-8846(89)90088-4

Gallé, C. (2001). Effect of drying on cement-based materials pore structure as identified by mercury intrusion porosimetry: A comparative study between oven-, vacuum-, and freeze-drying. *Cement and Concrete Research*, *31*(10), 1467–1477. doi:10.1016/S0008-8846(01)00594-4

Garboczi, E. J. (1990). Permeability, diffusivity, and microstructural parameters: A critical review. *Cement and Concrete Research*, *20*(4), 591–601. doi:10.1016/0008-8846(90)90101-3

Garcia-Lodeiro, I., Palomo, A., Fernández-Jiménez, A., & Macphee, D. E. (2011). Compatibility studies between N-A-S-H and C-A-S-H gels. Study in the ternary diagram Na2O–CaO–Al2O3–SiO2–H2O. *Cement and Concrete Research*, *41*(9), 923–931. doi:10.1016/j.cemconres.2011.05.006

Ghrici, M., Kenai, S., & Said-Mansour, M. (2007). Mechanical properties and durability of mortar and concrete containing natural pozzolana and limestone blended cements. *Cement and Concrete Composites*, *29*(7), 542–549. doi:10.1016/j.cemconcomp.2007.04.009

Githachuri, K., & Alexander, M. G. (2013). Durability performance potential and strength of blended Portland limestone cement concrete. *Cement and Concrete Composites*, *39*, 115–121. doi:10.1016/j.cemconcomp.2013.03.027

Gruber, K. A., Ramlochan, T., Boddy, A., Hooton, R. D., & Thomas, M. D. A. (2001). Increasing concrete durability with high-reactivity metakaolin. *Cement and Concrete Composites*, *23*(6), 479–484. doi:10.1016/S0958-9465(00)00097-4

Hendriks, C., Worrell, E., De Jager, D., Blok, K., & Riemer, P. (2002). Emission reduction of greenhouse gases from the cement industry. *International Energy Agency*.

Imbabi, M. S., Carrigan, C., & McKenna, S. (2012). Trends and developments in green cement and concrete technology. *International Journal of Sustainable Built Environment*, *1*(2), 194–216. doi:10.1016/j.ijsbe.2013.05.001

Ipavec, A., Vuk, T., Gabrovšek, R., & Kaučič, V. (2013). Chloride binding into hydrated blended cements: The influence of limestone and alkalinity. *Cement and Concrete Research*, *48*, 74–85. doi:10.1016/j.cemconres.2013.02.010

Irassar, E. F., Violini, D., Rahhal, V. F., Milanesi, C., Trezza, M. A., & Bonavetti, V. L. (2011). Influence of limestone content, gypsum content and fineness on early age properties of Portland limestone cement produced by inter-grinding. *Cement and Concrete Composites*, *33*(2), 192–200. doi:10.1016/j.cemconcomp.2010.10.001

Jain, J. A., & Neithalath, N. (2010). Chloride transport in fly ash and glass powder modified concretes – Influence of test methods on microstructure. *Cement and Concrete Composites*, *32*(2), 148–156. doi:10.1016/j.cemconcomp.2009.11.010

Jain, J., & Neithalath, N. (2011). Electrical impedance analysis based quantification of microstructural changes in concretes due to non-steady state chloride migration. *Materials Chemistry and Physics*, *129*(1–2), 569–579. doi:10.1016/j.matchemphys.2011.04.057

Jenq, Y., & Shah, S. (1985). Two Parameter Fracture Model for Concrete. *Journal of Engineering Mechanics*, *111*(10), 1227–1241. doi:10.1061/(ASCE)0733-9399(1985)111:10(1227)

Julio-Betancourt, G. A., & Hooton, R. D. (2004). Study of the Joule effect on rapid chloride permeability values and evaluation of related electrical properties of concretes. *Cement and Concrete Research*, *34*(6), 1007–1015. doi:10.1016/j.cemconres.2003.11.012

Kadri, E.-H., Kenai, S., Ezziane, K., Siddique, R., & De Schutter, G. (2011). Influence of metakaolin and silica fume on the heat of hydration and compressive strength development of mortar. *Applied Clay Science*, *53*(4), 704–708. doi:10.1016/j.clay.2011.06.008

Kar, A., Ray, I., Unnikrishnan, A., & Davalos, J. F. (2012). Estimation of C–S-H and calcium hydroxide for cement pastes containing slag and silica fume. *Construction and Building Materials*, *30*, 505–515. doi:10.1016/j.conbuildmat.2011.12.029

Khatri, R. P., Sirivivatnanon, V., & Gross, W. (1995). Effect of different supplementary cementitious materials on mechanical properties of high performance concrete. *Cement and Concrete Research*, *25*(1), 209–220. doi:10.1016/0008-8846(94)00128-L

Kumar, A., Oey, T., Kim, S., Thomas, D., Badran, S., Li, J., … Sant, G. (2013). Simple methods to estimate the influence of limestone fillers on reaction and property evolution in cementitious materials. *Cement and Concrete Composites*, *42*, 20–29. doi:10.1016/j.cemconcomp.2013.05.002

Lam, L., Wong, Y. L., & Poon, C. S. (2000). Degree of hydration and gel/space ratio of high-volume fly ash/cement systems. *Cement and Concrete Research*, *30*(5), 747–756. doi:10.1016/S0008-8846(00)00213-1

Liabastre, A. A., & Orr, C. (1978). An evaluation of pore structure by mercury penetration. *Journal of Colloid and Interface Science*, *64*(1), 1–18. doi:10.1016/0021-9797(78)90329-6

Lothenbach, B., Le Saout, G., Gallucci, E., & Scrivener, K. (2008). Influence of limestone on the hydration of Portland cements. *Cement and Concrete Research*, *38*(6), 848–860. doi:10.1016/j.cemconres.2008.01.002

Lu, X. (1997). Application of the Nernst-Einstein equation to concrete. *Cement and Concrete Research*, *27*(2), 293–302. doi:10.1016/S0008-8846(96)00200-1

Luo, R., Cai, Y., Wang, C., & Huang, X. (2003). Study of chloride binding and diffusion in GGBS concrete. *Cement and Concrete Research*, *33*(1), 1–7. doi:10.1016/S0008-8846(02)00712-3

Madandoust, R., & Mousavi, S. Y. (2012). Fresh and hardened properties of self-compacting concrete containing metakaolin. *Construction and Building Materials*, *35*, 752–760. doi:10.1016/j.conbuildmat.2012.04.109

Marsh, B. K., & Day, R. L. (1988). Pozzolanic and cementitious reactions of fly ash in blended cement pastes. *Cement and Concrete Research*, *18*(2), 301–310. doi:10.1016/0008-8846(88)90014-2

Marzouki, A., Lecomte, A., Beddey, A., Diliberto, C., & Ben Ouezdou, M. (2013). The effects of grinding on the properties of Portland-limestone cement. *Construction and Building Materials*, *48*, 1145–1155. doi:10.1016/j.conbuildmat.2013.07.053

Matschei, T., Lothenbach, B., & Glasser, F. P. (2007). The role of calcium carbonate in cement hydration. *Cement and Concrete Research*, *37*(4), 551–558. doi:10.1016/j.cemconres.2006.10.013

Menéndez, G., Bonavetti, V., & Irassar, E. F. (2003). Strength development of ternary blended cement with limestone filler and blast-furnace slag. *Cement and Concrete Composites*, *25*(1), 61–67. doi:10.1016/S0958-9465(01)00056-7

Moon, H. Y., Kim, H. S., & Choi, D. S. (2006). Relationship between average pore diameter and chloride diffusivity in various concretes. *Construction and Building Materials*, *20*(9), 725–732. doi:10.1016/j.conbuildmat.2005.02.005

Moro, F., & Böhni, H. (2002). Ink-Bottle Effect in Mercury Intrusion Porosimetry of Cement-Based Materials. *Journal of Colloid and Interface Science*, *246*(1), 135–149. doi:10.1006/jcis.2001.7962

Neithalath, N., Persun, J., & Hossain, A. (2009). Hydration in high-performance cementitious systems containing vitreous calcium aluminosilicate or silica fume. *Cement and Concrete Research*, *39*(6), 473–481. doi:10.1016/j.cemconres.2009.03.006

Neithalath, N., Weiss, J., & Olek, J. (2006). Characterizing Enhanced Porosity Concrete using electrical impedance to predict acoustic and hydraulic performance. *Cement and Concrete Research*, *36*(11), 2074–2085. doi:10.1016/j.cemconres.2006.09.001

Nochaiya, T., Wongkeo, W., & Chaipanich, A. (2010). Utilization of fly ash with silica fume and properties of Portland cement–fly ash–silica fume concrete. *Fuel*, *89*(3), 768–774. doi:10.1016/j.fuel.2009.10.003

NT Build 492. Concrete, Mortar and Cement-Based Repair Materials: Chloride Migration Coeffecient from Non-Steady-State Migration Experiments. (1990). *Nord Test Method (1999)*.

Oey, T., Kumar, A., Bullard, J. W., Neithalath, N., & Sant, G. (2013). The Filler Effect: The Influence of Filler Content and Surface Area on Cementitious Reaction Rates. *Journal of the American Ceramic Society*, *96*(6), 1978–1990. doi:10.1111/jace.12264

Oggioni, G., Riccardi, R., & Toninelli, R. (2011). Eco-efficiency of the world cement industry: A data envelopment analysis. *Energy Policy*, *39*(5), 2842–2854. doi:10.1016/j.enpol.2011.02.057

Paiva, H., Velosa, A., Cachim, P., & Ferreira, V. M. (2012). Effect of metakaolin dispersion on the fresh and hardened state properties of concrete. *Cement and Concrete Research*, *42*(4), 607–612. doi:10.1016/j.cemconres.2012.01.005

Pelletier-Chaignat, L., Winnefeld, F., Lothenbach, B., & Müller, C. J. (2012). Beneficial use of limestone filler with calcium sulphoaluminate cement. *Construction and Building Materials*, *26*(1), 619–627. doi:10.1016/j.conbuildmat.2011.06.065

Perlot, C., Rougeau, P., & Dehaudt, S. (2013). Slurry of metakaolin combined with limestone addition for self-compacted concrete. Application for precast industry. *Cement and Concrete Composites*, *44*, 50–57. doi:10.1016/j.cemconcomp.2013.07.003

Pipilikaki, P., & Beazi-Katsioti, M. (2009). The assessment of porosity and pore size distribution of limestone Portland cement pastes. *Construction and Building Materials*, *23*(5), 1966–1970. doi:10.1016/j.conbuildmat.2008.08.028

Poon, C.-S., Lam, L., Kou, S. C., Wong, Y.-L., & Wong, R. (2001). Rate of pozzolanic reaction of metakaolin in high-performance cement pastes. *Cement and Concrete Research*, *31*(9), 1301–1306. doi:10.1016/S0008-8846(01)00581-6

Qian, X., & Li, Z. (2001). The relationships between stress and strain for high-performance concrete with metakaolin. *Cement and Concrete Research*, *31*(11), 1607–1611. doi:10.1016/S0008-8846(01)00612-3

Rehan, R., & Nehdi, M. (2005). Carbon dioxide emissions and climate change: policy implications for the cement industry. *Environmental Science & Policy*, *8*(2), 105–114. doi:10.1016/j.envsci.2004.12.006

Richardson, I. G. (1999). The nature of C-S-H in hardened cements. *Cement and Concrete Research*, *29*(8), 1131–1147. doi:10.1016/S0008-8846(99)00168-4

Sakai, Y., Nakamura, C., & Kishi, T. (2014). Evaluation of mass transfer resistance of concrete based on representative pore size of permeation resistance. *Construction and Building Materials*, *51*, 40–46. doi:10.1016/j.conbuildmat.2013.10.037

Samson, E., Marchand, J., & Snyder, K. A. (2003). Calculation of ionic diffusion coefficients on the basis of migration test results. *Materials and Structures*, *36*, 156–165.

Sánchez, I., Nóvoa, X. R., de Vera, G., & Climent, M. A. (2008). Microstructural modifications in Portland cement concrete due to forced ionic migration tests. Study by impedance spectroscopy. *Cement and Concrete Research*, *38*(7), 1015–1025. doi:10.1016/j.cemconres.2008.03.012

Sanish, K. B., Neithalath, N., & Santhanam, M. (2013). Monitoring the evolution of material structure in cement pastes and concretes using electrical property measurements. *Construction and Building Materials*, *49*, 288–297. doi:10.1016/j.conbuildmat.2013.08.038

Schneider, M., Romer, M., Tschudin, M., & Bolio, H. (2011). Sustainable cement production—present and future. *Cement and Concrete Research*, *41*(7), 642–650. doi:10.1016/j.cemconres.2011.03.019

Schwarz, N., & Neithalath, N. (2008). Influence of a fine glass powder on cement hydration: Comparison to fly ash and modeling the degree of hydration. *Cement and Concrete Research*, *38*(4), 429–436. doi:10.1016/j.cemconres.2007.12.001

Shekarchi, M., Bonakdar, A., Bakhshi, M., Mirdamadi, A., & Mobasher, B. (2010). Transport properties in metakaolin blended concrete. *Construction and Building Materials*, *24*(11), 2217–2223. doi:10.1016/j.conbuildmat.2010.04.035

Shi, C. (2004). Effect of mixing proportions of concrete on its electrical conductivity and the rapid chloride permeability test (ASTM C1202 or ASSHTO T277) results. *Cement and Concrete Research*, *34*(3), 537–545. doi:10.1016/j.cemconres.2003.09.007

Shi, D., & Winslow, D. N. (1985). Contact angle and damage during mercury intrusion into cement paste. *Cement and Concrete Research*, *15*(4), 645–654. doi:10.1016/0008-8846(85)90064-X

Shoude, W., Cheng, C., Lingchao, L., & Xin, C. (2012). Effects of slag and limestone powder on the hydration and hardening process of alite-barium calcium sulphoaluminate cement. *Construction and Building Materials*, *35*, 227–231. doi:10.1016/j.conbuildmat.2012.03.004

Snyder, K. A., Feng, X., Keen, B. D., & Mason, T. O. (2003). Estimating the electrical conductivity of cement paste pore solutions from OH−, K+ and Na+ concentrations. *Cement and Concrete Research*, *33*(6), 793–798. doi:10.1016/S0008-8846(02)01068-2

Song, G. (2000). Equivalent circuit model for AC electrochemical impedance spectroscopy of concrete. *Cement and Concrete Research*, *30*(11), 1723–1730. doi:10.1016/S0008-8846(00)00400-2

Spiesz, P., Ballari, M. M., & Brouwers, H. J. H. (2012). RCM: A new model accounting for the non-linear chloride binding isotherm and the non-equilibrium conditions between the free- and bound-chloride concentrations. *Construction and Building Materials*, *27*(1), 293–304. doi:10.1016/j.conbuildmat.2011.07.045

Spiesz, P., & Brouwers, H. J. H. (2012). Influence of the applied voltage on the Rapid Chloride Migration (RCM) test. *Cement and Concrete Research*, *42*(8), 1072–1082. doi:10.1016/j.cemconres.2012.04.007

Stanish, K., Hooton, R. D., & Thomas, M. D. A. (2004). A novel method for describing chloride ion transport due to an electrical gradient in concrete: Part 1. Theoretical description. *Cement and Concrete Research*, *34*(1), 43–49. doi:10.1016/S0008-8846(03)00191-1

Streicher, P. E., & Alexander, M. G. (1995). A chloride conduction test for concrete. *Cement and Concrete Research*, *25*(6), 1284–1294. doi:10.1016/0008-8846(95)00121-R

Tang, L. (1999). Concentration dependence of diffusion and migration of chloride ions: Part 1. Theoretical considerations. *Cement and Concrete Research*, *29*(9), 1463–1468. doi:10.1016/S0008-8846(99)00121-0

Taylor, H. F. W. (1987). A method for predicting alkali ion concentrations in cement pore solutions. *Advanced Cement Research*, *1*, 5–16.

Tong, L., & Gjørv, O. E. (2001). Chloride diffusivity based on migration testing. *Cement and Concrete Research*, *31*(7), 973–982. doi:10.1016/S0008-8846(01)00525-7

Vance, K., Aguayo, M., Oey, T., Sant, G., & Neithalath, N. (2013). Hydration and strength development in ternary portland cement blends containing limestone and fly ash or metakaolin. *Cement and Concrete Composites*, *39*, 93–103. doi:10.1016/j.cemconcomp.2013.03.028

Washburn, E. W. (1921). Note on a Method of Determining the Distribution of Pore Sizes in a Porous Material. *Proceedings of the National Academy of Sciences of the United States of America*, *7*(4), 115–116.

Worrell, E. (2014). Cement and Energy. In *Reference Module in Earth Systems and Environmental Sciences*. Elsevier. Retrieved from http://www.sciencedirect.com/science/article/pii/B9780124095489090576

Worrell, E., Martin, N., & Price, L. (2000). Potentials for energy efficiency improvement in the US cement industry. *Energy*, *25*(12), 1189–1214. doi:10.1016/S0360-5442(00)00042-6

Xu, J., Jiang, L., & Wang, J. (2009). Influence of detection methods on chloride threshold value for the corrosion of steel reinforcement. *Construction and Building Materials*, *23*(5), 1902–1908. doi:10.1016/j.conbuildmat.2008.09.011

Yu, Z., & Ye, G. (2013). The pore structure of cement paste blended with fly ash. *Construction and Building Materials*, *45*, 30–35. doi:10.1016/j.conbuildmat.2013.04.012

Zeng, Q., Li, K., Fen-chong, T., & Dangla, P. (2012). Determination of cement hydration and pozzolanic reaction extents for fly-ash cement pastes. *Construction and Building Materials*, *27*(1), 560–569. doi:10.1016/j.conbuildmat.2011.07.007

Zeng, Q., Li, K., Fen-Chong, T., & Dangla, P. (2012). Analysis of pore structure, contact angle and pore entrapment of blended cement pastes from mercury porosimetry data. *Cement and Concrete Composites*, *34*(9), 1053–1060. doi:10.1016/j.cemconcomp.2012.06.005

Zhang, Y. M., Sun, W., & Yan, H. D. (2000). Hydration of high-volume fly ash cement pastes. *Cement and Concrete Composites*, *22*(6), 445–452. doi:10.1016/S0958-9465(00)00044-5

Zhang, Z., Provis, J. L., Reid, A., & Wang, H. (2014). Geopolymer foam concrete: An emerging material for sustainable construction. *Construction and Building Materials*, *56*, 113–127. doi:10.1016/j.conbuildmat.2014.01.081